CONVERGENCE ANALYSIS OF THE GENERALIZED FINITE ELEMENT METHOD WITH GLOBAL-LOCAL ENRICHMENTS

BY

VARUN GUPTA

THESIS

Submitted in partial fulfillment of the requirements
for the degree of Master of Science in Civil Engineering
in the Graduate College of the
University of Illinois at Urbana-Champaign, 2010

Urbana, Illinois

Adviser:

Professor C. Armando Duarte

Abstract

The global-local analysis procedure in the Finite Element Method is broadly used in industry for the analysis of cracks or localized stress concentrations in large, complex, three-dimensional domains. However, the limitations of this technique are well-known. The global-local FEM (*GL-FEM*) involves two steps: First, the solution of the given problem is computed on a coarse, global, quasi-uniform mesh, in which the cracks or other local features need not be discretized. The solution of this problem is then used as boundary conditions to solve another Finite Element problem, which is basically a local sub-domain, comprised of localized features (like cracks), extracted from the global domain.The efficacy of the so-called Generalized Finite Element Method (*GFEM*) in solving such multi-scale problems has been quite well proven in past few years. Therefore, combining the two approaches, going one step further from Global-Local Finite Element Analysis, and using the local solution as an enrichment function for the global problem through the Partition of Unity framework of the Generalized Finite Element Method, gives rise to the Generalized Finite Element Method with global-local enrichments (or $GFEM^{g\text{-}l}$).

As these classes of methods are relatively new, there are many issues which need to be addressed to make these methods robust enough for their industrial applicability in a comprehensive manner. One of the issues surrounding this $GFEM^{g\text{-}l}$ approach concerns the domain size of the local problem containing the complex localized features of a structural problem, and the focus of this study is to provide guidance to address this issue.

This study focuses on coming up with guidelines for selecting the size of the enrichment zone for three-dimensional fracture mechanics problems. A theoretical proof and rigorous convergence studies are presented here to provide the guidelines for selecting the size of enrichment zone for practical problems. The effect of inexact boundary conditions, applied to the local problem, on the solution is also investigated.

Acknowledgments

I am thankful to my advisor, Prof. C. Armando Duarte, for his guidance, support and critiques which helped me in the development of this work. I would also like to express my appreciation to Air Force Office of Scientific Research for providing me with the financial support.

Finally, thanks to my friends and colleagues for the support and encouragement they provided me, which helped me all the way through this process.

Table of Contents

List of Figures . . . . . **v**

Chapter 1 Introduction **1**
1.1 Generalized Finite Element Approximations 1
1.2 Generalized Finite Element Method with global-local enrichments ($GFEM^{g\text{-}l}$) 2
1.2.1 Formulation of Global Problem 3
1.2.2 Local Problem 4
1.2.3 Global-Local Enrichment Functions 4
1.3 Objectives and Outline 5

Chapter 2 Size of Enrichment Zone **7**
2.1 Types of Enrichment 7
2.1.1 Topological Enrichment 7
2.1.2 Geometrical Enrichment 7
2.2 Optimal Size of Enrichment Zone 8
2.3 Model Problem: Edge-Crack Panel 12
2.4 Optimal Local Problem Refinement 15
2.5 Effect of Enrichment Zone Size 21

Chapter 3 Effect of inexact Boundary Conditions **39**
3.1 Theoretical estimate of the Error in Boundary Condition 40
3.2 Numerical Studies and Discussion 44

Chapter 4 Concluding Remarks **50**

Chapter 5 References **51**

List of Figures

1.1 Construction of GFEM shape functions . . . 2
1.2 Figure showing the construction of GFEM shape functions using global-local enrichments . . . 3

2.1 Topological Enrichment . . . 7
2.2 Geometrical Enrichment . . . 8
2.3 Figure showing behavior of the solution near a crack tip . . . 9
2.4 Model problem with a through-the-thickness crack . . . 12
2.5 Initial meshes used for the study . . . 14
2.6 Figure showing the extraction of a localized geometric domain from global mesh to obtain the local mesh . . . 16
2.7 Convergence behavior plotted with respect to the local element size for Mesh 1 . . . 16
2.8 Convergence behavior plotted with respect to the local element size for Mesh 2 ($nref_{uniform} = 0$) . . . 17
2.9 Convergence behavior plotted with respect to the local element size for Mesh 2 ($nref_{uniform} = 1$) . . . 18
2.10 Convergence behavior plotted with respect to the local element size for Mesh 3 . . . 18
2.11 Convergence behavior plotted with respect to the local element size for Mesh 4 . . . 19
2.12 Convergence behavior plotted with respect to the local element size for all the four meshes . . . 20
2.13 Figure showing different enrichment zones and local problem . . . 22
2.14 *GFEM*$^{\text{g-l}}$ Meshes 1 and 2 . . . 23
2.15 *GFEM*$^{\text{g-l}}$ Meshes 3 and 4 . . . 24
2.16 Convergence plots showing *GFEM*$^{\text{g-l}}$ results . . . 25
2.17 Figure showing the effect of local refinement on the global problem convergence behavior . . . 27
2.18 Figure showing the effect of using branch-function enrichment in the local problem . . . 27
2.19 Figure showing the comparison between the cases with and without branch-function enrichment in the local problem . . . 28
2.20 Convergence behavior plotted with respect to the Number of Enrichment Degrees of Freedom . . . 31
2.21 Figure showing the effect of Local refinement on the Global behavior with different enrichment zone sizes . . . 33
2.22 Convergence of Stress Intensity Factors . . . 35
2.23 Meshes used for studying results from *hp-GFEM* . . . 36
2.24 Convergence plots showing *hp-GFEM* results . . . 37
2.25 Convergence plots showing *hp-GFEM* and *GFEM*$^{\text{g-l}}$ results . . . 38

3.1 Figure showing the process of solving a crack growth problem with the help of *GFEM*$^{\text{g-l}}$ . . . 39
3.2 Figure showing coordinate system representation for cracks of size $(2a)$ and $(2a+2\Delta a)$ for an infinite plate loaded at infinity. . . . 40
3.3 Figure showing the variation of error in BC with the crack step size Δa . . . 42
3.4 Figure showing the variation of error in BC with crack step scaled by the size of $S_2\left(\frac{\Delta a}{r_2}\right)$ . . . 43
3.5 Edge-crack panel showing different locations of crack front to study the effect of inexact Boundary Conditions . . . 44
3.6 Figure showing local problem domains solved with two different boundary conditions . . . 45

3.7 Figure showing the global and local problem meshes used for studying the effect of inexact Boundary Conditions 47
3.8 Figure showing the relative error in Strain Energy of Local Problem plotted against crack step size Δa 48
3.9 Figure showing the relative error in Strain Energy of Local Problem plotted against a scaled parameter, $\frac{\Delta a}{r}$ 48
3.10 Figure showing the relative error in Strain Energy of Enriched Global Problem plotted against crack step size Δa 49
3.11 Figure showing the relative error in Strain Energy of Enriched Global Problem plotted against $\frac{\Delta a}{r}$ . . 49

Chapter 1

Introduction

The global-local Finite Element Analysis is a broadly used tool in the industry for solving multi-scale problems, but the problems associated with this technique are well-known and therefore several improvements to these methods have been proposed in the past by different researchers [13, 29]. The effectiveness of the *hp*-clouds method [7, 10–12, 19], Generalized FEM [2, 3, 17] and Extended FEM [6, 18], all of which are based on the Partition of Unity methods [2, 12], in solving multi-scale problems with localized features of interest, has been well established in recent past. The above-mentioned methods, however, rely on closed-form analytical enrichment functions and it is not always possible to have the analytical expressions for the enrichment functions, which offsets some of the advantages associated with these methods for certain problems. This lead to the development of Generalized Finite Element method with global-local enrichments (*GFEM*$^{\text{g-l}}$) [8, 14, 15], which combines the classical global-local finite element method with the partition of unity approach. It involves the solution of a local boundary value problem using boundary conditions from the solution of the global problem discretized with the coarse scale elements. These local solutions are in turn used to enrich the solution space of the coarse global problem with the help of the Partition of Unity framework. The local problems can be accurately solved using the *hp-GFEM* and therefore this approach does not rely on analytical solutions. These global-local enrichment functions can also be used in other class of problems, as demonstrated in [20], for problems having sharp thermal gradients. Many other advantages and the implementation issues related to these methods have been discussed in [8, 14, 15]. The following sections provide the brief review of the Generalized Finite Element Method, followed by the global-local approach to build the enrichment functions.

1.1 Generalized Finite Element Approximations

This section deals with a brief review of the Generalized Finite Element Methods; further details can be found in [2, 9, 19, 26]. The shape functions, $\phi_{\alpha i}$, in this class of methods are built from the product of a partition of unity, φ_α, and enrichment functions, $L_{\alpha i}$ and are defined as:

$$\phi_{\alpha i} := \varphi_\alpha L_{\alpha i} \qquad i \in \mathscr{I}(\alpha) \qquad \text{(no summation on } \alpha\text{)} \tag{1.1}$$

where $\varphi_\alpha,\ \alpha = 1,\ldots,N$, ($N$ being the number of functions), constitute a partition of unity. The index set of the enrichment functions at a vertex node $\boldsymbol{x}_\alpha$ is denoted by $\mathscr{I}(\alpha)$. In the generalized finite element method, the partition of unity is, in general, provided by the standard linear Lagrangian finite element shape functions and thus the support of φ_α, denoted by ω_α, is then given by the union of all the finite elements sharing a vertex node $\boldsymbol{x}_\alpha$. The resulting shape functions are called generalized finite element shape functions. Figure 1.1 illustrates the construction of GFEM shape functions. When polynomial functions are used for enrichment functions, $L_{\alpha i}$, the solution space spanned by generalized FEM becomes equivalent to that of standard FEM, however the main strength of these methods comes from the fact that it can even use any non-polynomial enrichment functions (which can represent the solution of a given problem) as illustrated in Figure 1.1(b).

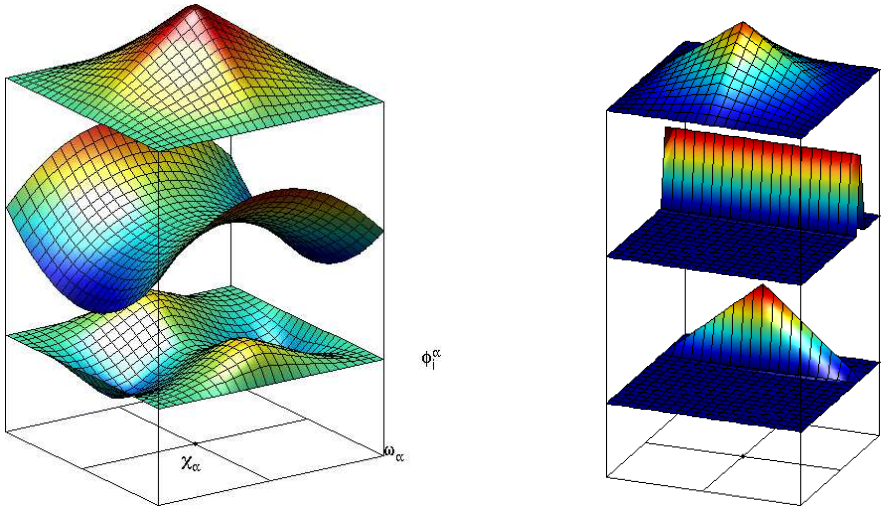

Figure 1.1: *Construction of a generalized FEM shape function using a polynomial (a) and a non-polynomial enrichment (b). Here, φ_α is the function at the top, the enrichment function, $L_{\alpha i}$, is the function in the middle, and the generalized FE shape function, $\phi_{\alpha i}$, is the resulting shape function shown at bottom.*

1.2 Generalized Finite Element Method with global-local enrichments (*GFEM*$^{\text{g-l}}$)

This section briefly reviews the global-local approach to build the enrichment functions for the Generalized FEM; details can be found in [8, 14, 15]. The *GFEM*$^{\text{g-l}}$ is nothing but the Generalized Finite Element Method wherein the enrichment functions are built from the numerical solution of a Local Boundary Value Problem. It involves the solution of a local boundary value problem using the boundary conditions from a coarse scale global problem, and then these local solutions are in turn used to paste the characteristics of the localized features of the problem, in the

coarse scale global space with the help of global-local enrichment functions (as shown in Figure 1.2). Though the formulation of this methodology provided below, focuses on three-dimensional elasticity problems, the formulation is applicable for other class of problems as well.

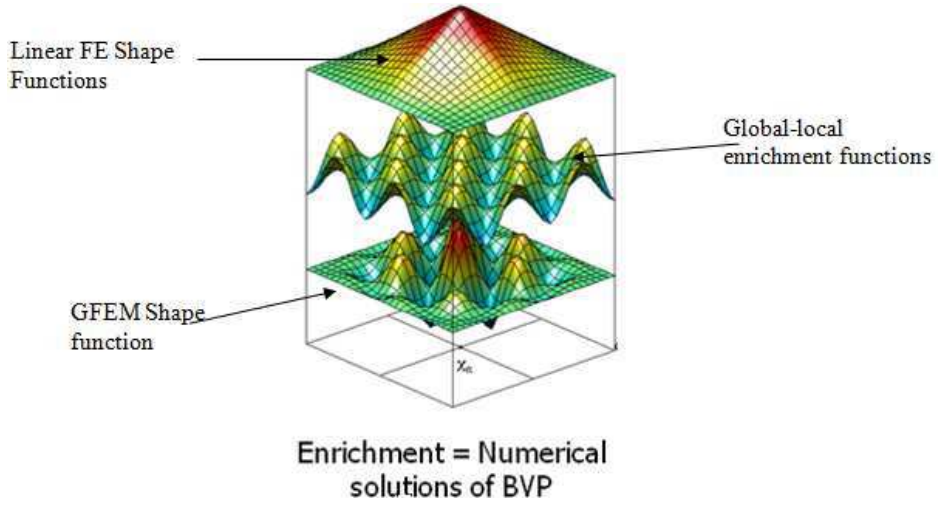

Figure 1.2: *Figure showing the construction of GFEM shape functions using global-local enrichments*

1.2.1 Formulation of Global Problem

Consider a domain, $\bar{\Omega}_G = \Omega_G \cup \partial\Omega_G$ in $\boldsymbol{R}^3$, where the bar indicates that the boundary is inclusive in the domain. The boundary is decomposed as $\partial\Omega_G = \partial\Omega_G^u \cup \partial\Omega_G^\sigma$ with $\partial\Omega_G^u \cap \partial\Omega_G^\sigma = \emptyset$.

The equilibrium and constitutive equations are given by

$$\nabla \cdot \boldsymbol{\sigma} = \boldsymbol{0} \qquad \boldsymbol{\sigma} = \boldsymbol{C} : \boldsymbol{\varepsilon} \qquad \text{in } \Omega_G, \tag{1.2}$$

where $\boldsymbol{C}$ is Hooke's tensor, $\boldsymbol{\sigma}$ denotes the Cauchy stress tensor and $\boldsymbol{\varepsilon}$ is the strain tensor. The following boundary conditions are prescribed on $\partial\Omega_G$

$$\boldsymbol{u} = \bar{\boldsymbol{u}} \text{ on } \partial\Omega_G^u \qquad \boldsymbol{\sigma} \cdot \boldsymbol{n} = \bar{\boldsymbol{t}} \text{ on } \partial\Omega_G^\sigma, \tag{1.3}$$

where $\boldsymbol{n}$ is the outward unit normal vector to $\partial\Omega_G^\sigma$ and $\bar{\boldsymbol{t}}$ and $\bar{\boldsymbol{u}}$ are prescribed tractions and displacements, respectively. Equations (1.2) and (1.3) are the strong form of governing equations. Let $\boldsymbol{u}_G^0$ denote a generalized FEM approximation of the exact solution $\boldsymbol{u}$ of the problem statement given by equations (1.2) and (1.3). From the Principle of Virtual Work, it can be derived that the approximation $\boldsymbol{u}_G^0$ will be the solution of the following problem:

Find $\boldsymbol{u}_G^0 \in \boldsymbol{X}_G^{hp}(\Omega_G) \subset H^1(\Omega_G)$ such that, $\forall\, \boldsymbol{v}_G^0 \in \boldsymbol{X}_G^{hp}(\Omega_G)$

$$\int_{\Omega_G} \boldsymbol{\sigma}(\boldsymbol{u}_G^0) : \boldsymbol{\varepsilon}(\boldsymbol{v}_G^0) d\boldsymbol{x} + \eta \int_{\partial\Omega_G^u} \boldsymbol{u}_G^0 \cdot \boldsymbol{v}_G^0 d\boldsymbol{s} = \int_{\partial\Omega_G^\sigma} \bar{\boldsymbol{t}} \cdot \boldsymbol{v}_G^0 d\boldsymbol{s} + \eta \int_{\partial\Omega_G^u} \bar{\boldsymbol{u}} \cdot \boldsymbol{v}_G^0 d\boldsymbol{s} \tag{1.4}$$

where, $\boldsymbol{X}_G^{hp}(\Omega_G)$ is a discretization of $H^1(\Omega_G)$, the Hilbert space defined on Ω_G, built with generalized FEM shape functions and η is a penalty parameter. Discretization for solving problem (1.4) is typically performed with the help of a coarse quasi-uniform finite element mesh which leads to a system of linear equations to be solved for the unknown degrees of freedom of $\boldsymbol{u}_G^0$.

1.2.2 Local Problem

Let Ω_{loc} denotes a *local domain*, which is extracted from Ω_G and may contain cracks, holes, inclusions, fibers, or other local features of interest. The following is the weak form of the local problem which is solved on Ω_{loc} after the global solution $\boldsymbol{u}_G^0$ is computed as described above:

Find $\boldsymbol{u}_{loc} \in \boldsymbol{X}_{loc}^{hp}(\Omega_{loc}) \subset H^1(\Omega_{loc})$ such that, $\forall\, \boldsymbol{v}_{loc} \in \boldsymbol{X}_{loc}^{hp}(\Omega_{loc})$

$$\begin{aligned}
&\int_{\Omega_{loc}} \boldsymbol{\sigma}(\boldsymbol{u}_{loc}) : \boldsymbol{\varepsilon}(\boldsymbol{v}_{loc}) d\boldsymbol{x} + \eta \int_{\partial\Omega_{loc}\setminus(\partial\Omega_{loc}\cap\partial\Omega_G^\sigma)} \boldsymbol{u}_{loc} \cdot \boldsymbol{v}_{loc} d\boldsymbol{s} = \\
&\eta \int_{\partial\Omega_{loc}\setminus(\partial\Omega_{loc}\cap\partial\Omega_G)} \boldsymbol{u}_G^0 \cdot \boldsymbol{v}_{loc} d\boldsymbol{s} + \eta \int_{\partial\Omega_{loc}\cap\partial\Omega_G^u} \bar{\boldsymbol{u}} \cdot \boldsymbol{v}_{loc} d\boldsymbol{s} + \int_{\partial\Omega_{loc}\cap\partial\Omega_G^\sigma} \bar{\boldsymbol{t}} \cdot \boldsymbol{v}_{loc} d\boldsymbol{s}
\end{aligned} \tag{1.5}$$

where, $\boldsymbol{X}_{loc}^{hp}(\Omega_{loc})$ is a discretization of $H^1(\Omega_{loc})$ using GFEM shape functions. Problem statement (1.5) uses the solution of the global problem (Section 1.2.1), $\boldsymbol{u}_G^0$, as boundary condition on $\partial\Omega_{loc}\setminus(\partial\Omega_{loc}\cap\partial\Omega_G)$. Exact boundary conditions are prescribed on portions of $\partial\Omega_{loc}$ that intersect either $\partial\Omega_G^u$ or $\partial\Omega_G^\sigma$.

1.2.3 Global-Local Enrichment Functions

Using Equation 1.1 and the concept explained through Figure 1.2, the Generalized FEM shape function can be modified as,

$$\boldsymbol{\phi}_\alpha = \varphi_\alpha \boldsymbol{u}_{loc} \tag{1.6}$$

where $\boldsymbol{u}_{loc}$ is the local solution obtained in Section 1.2.2 and is also called as a global-local enrichment function in the context of $GFEM^{\text{g-l}}$. This shape function is used at node $\boldsymbol{x}_\alpha$ of the global mesh whose support, ω_α, is contained in the local domain Ω_{loc}. The global problem defined initially in Section 1.2.1 is then solved again with the solution space now modified to include the global-local enrichment shape functions, and is called as Enriched Global Problem whose solution is denoted by $\boldsymbol{u}_G^E$.

1.3 Objectives and Outline

There are certain issues associated with these GFEM methods, which should be addressed before these can be widely accepted in the industry. A major issue in this *GFEM*$^{g\text{-}l}$ approach is to come up with some guidelines to help a user to choose the domain size of the local problem containing the local features of interest, like cracks, voids, inclusions etc. The domain size of the local problem, in turn, can be seen as being dependent on two broadly classified issues:

(i) **Effect of inexact BCs on the Local Boundary Value Problem**: For a general problem solved by the approach of *GFEM*$^{g\text{-}l}$, the boundary conditions for the local Boundary Value Problem (BVP) will be obtained from the solution of the initial global, coarse scale BVP. The solution of the initial global problem solved on a coarse scale mesh would not be accurate because the localized features are not modeled in this initial global problem. This will result in the inexact Boundary Conditions on the Local BVP. Now, it is known and can be intuitively concluded from Saint Venants principle that the effect of those inexact boundary conditions on the solution of the local BVP would get abated as the domain size of the local Boundary Value Problem is increased. Therefore, the bigger the local problem domain, the better it would be in terms of using inexact boundary conditions for the local BVP. But, on the other hand, increasing the size of the local problem, would increase the computational cost significantly, as a highly refined mesh is used in the local problem to capture the localized characteristics, and that would subside the whole advantage of using the Global-Local approach. So, there is a kind of trade-off in selecting the domain size of the local problem and the user should be able to balance out the above mentioned factors based on the problem at hand.

(ii) **Size of the Enrichment Zone**: In the context of *GFEM*$^{g\text{-}l}$, basically, what an enrichment zone means is the geometric zone (or region) of the global problem within which the solution of the local problem is used to enrich the global space with the global-local enrichment functions. In principle, the size of the enrichment zone can be as big as the domain size of the local problem. There are a few things though, which should be considered while selecting the size of the enrichment zone:

   (a) The enrichment zone should be big enough to be able to capture the localized features sufficiently (it is a relative term and will be discussed later in detail).

   (b) As also mentioned in the discussion above, for a general problem, the boundary conditions for the local BVP would be inexact, and the effect of those *bad* BCs would be more prominent, resulting in a poor solution close to the boundary. So, we would not want to include that poor solution while generating our global-local enrichment functions.

   (c) Computational cost: The bigger the size of the enrichment zone, the more would be the computational cost involved with it.

This study aims on providing guidelines to select the domain size of the local problem. Therefore, in that direction, based on the discussion above, Chapter 2 focuses on coming up with an optimal size of the enrichment zone so as to help moving one step further in selecting the domain size of the local problem. The effect of inexact BCs is not included in this chapter, so as to only vary one parameter at a time. Also, for now, we are only going to consider 'point (a)' (mentioned above), and would not look into the effect of inexact BCs on the size of enrichment zone, as talked about in 'point (b)'. And the goal of this chapter will be to provide directions for selecting an enrichment zone size big enough to be able to capture the localized features sufficiently, which is a relative term, so the solution would be deemed to qualify as sufficient, if we are able to get the optimal convergence rates with respect to the element size in the global problem with the uniform mesh refinement in the coarse scale global problem. Chapter 3 deals with studying the effect of inexact boundary conditions on the solution of the local problem and the enriched global problem. Though this study is focused on the three-dimensional linear elasticity problems, the results and conclusions from this study would be applicable for other class of problems as well, where these methods are applicable. And, further in this study, everything would be discussed in context of 3-D Fracture Mechanics problems. Finally, Chapter 4 summarizes the discussions, results and important points from chapters 2 and 3.

Chapter 2

Size of Enrichment Zone

2.1 Types of Enrichment

With respect to the domain of the enrichment region, it can be classified into two broad categories [5]:

2.1.1 Topological Enrichment

In this type of enrichment, only the elements which are cut by the crack front are enriched with the solution of the local problem. So, intuitively we can say that we are capturing only the characteristics of the solution at the crack front, but how significantly, is the point that still needs to be answered. This type of strategy is not good [16] (as we will also see later from the numerical results) and leads to poor convergence rates.

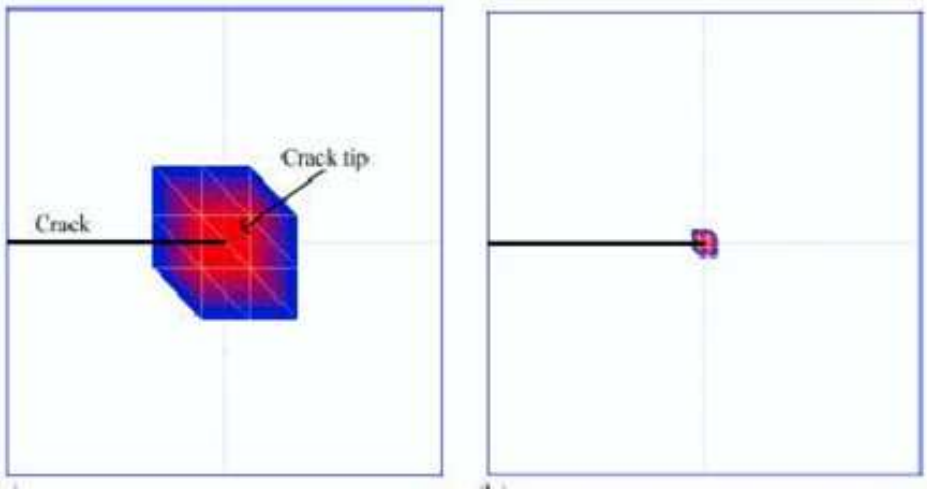

Figure 2.1: *Topological Enrichment*

2.1.2 Geometrical Enrichment

In this type of enrichment, all the nodes lying within a geometric region of radius d around the crack front are enriched with the solution of the local problem. Thus, as a result, we can capture the solution characteristics at the crack front

and in the nearby region as well. But this may lead to a large number of degrees of freedom (DOFs) in the enriched coarse scale global problem. So, it becomes important to choose the optimal size of the enrichment zone which is just big enough to obtain the optimal convergence behavior.

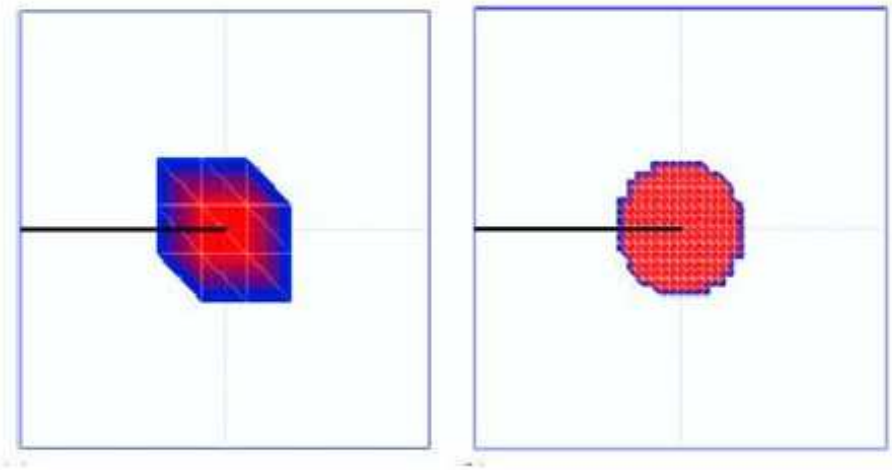

Figure 2.2: *Geometrical Enrichment*

2.2 Optimal Size of Enrichment Zone

As the finite element solution minimizes the strain energy of the error, the strain energy of the error is a logical measure of the overall quality of the finite element solution. The energy norm of the error of the finite element solution is governed by the following equation [27]:

$$\|e\|_{H^1(\Omega)} \leq Ch^{min(p,k-1)}\|u\|_{H^k(\Omega)} \tag{2.1}$$

where,

$\|e\|_{H^1(\Omega)}$ indicates the error in the energy norm,

'u' denotes the solution vector

'C' is a constant independent of u and h (unknown)

'h' is the size of the largest finite element in the mesh

'p' is the polynomial order of the elements

'k' denotes the order of the Hilbert space ($H^k(\Omega)$) to which the exact solution belongs, which in turn is a measure of the smoothness of the solution u

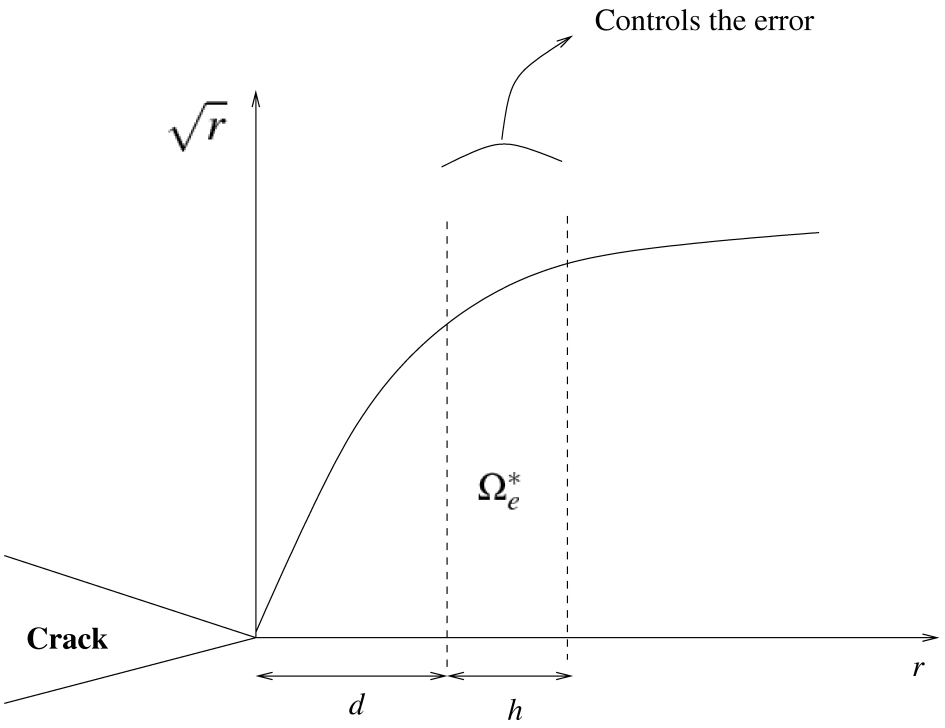

Figure 2.3: *Figure showing behavior of the solution near a crack tip*

Figure 2.3 shows the behavior of the Mode I expansion of the elasticity solution (which is proportional to $\sqrt{r}$) near a crack tip. The *x-axis* in the figure indicates the distance 'r' from the crack tip and '$\sqrt{r}$' is plotted on the *y-axis*. In Figure 2.3, the domain Ω_e^* contains all the elements ('h' denotes the size of these elements), which control the error, after the error within the enrichment zone of radius d is being taken care of sufficiently, by the enrichment functions.

Therefore, it means that the convergence of the GFEM solution is controlled by the error on Ω_e^*, as we know that on the elements farther away, the solution is smooth enough to yield the optimal convergence in the *h*-version of FEM.

From Equation (2.1), it can be seen that if the solution 'u' belongs to the Hilbert space of order '$p+1$' or larger, then the convergence rate would be governed by the polynomial order 'p' and will be the optimal convergence rate.

As, Ω_e^* controls the error, therefore for optimal convergence,

$$u|_{\Omega_e^*} \in H^{(p+1)}(\Omega_e^*) \tag{2.2}$$

Using equations (2.1)and (2.2), we get,

$$\|e\|_{H^1(\Omega_e^*)} \leq C_1 h^p \left[\|u\|_{H^{p+1}(\Omega_e^*)}\right] \tag{2.3}$$

Equation (2.3) in itself implies that the convergence rate will be optimal and would be equal to 'p', if the quantity in the square brackets is bounded by a constant.

By taking square on both sides of Equation (2.3), it can be written as,

$$\|e\|^2_{H^1(\Omega^*_e)} \leq Ch^{2p}\left[\|u\|^2_{H^{p+1}(\Omega^*_e)}\right] \tag{2.4}$$

Note that, as and when further constants appear while solving the inequality, those can be lumped into a single constant 'C'.

Now, we know that the solution near the singularity due to a crack is given by,

$$u(r,\theta) = r^{\frac{1}{2}} f(\theta) \tag{2.5}$$

where, 'r' is the distance from the crack tip and $f(\theta)$ is a smooth function of the angle θ formed between the location vector and the coordinate axis.

Taking $(p+1)^{th}$ derivative of Equation (2.5) with respect to 'r', we get,

$$\frac{\partial^{p+1} u}{\partial r^{p+1}} \approx r^{\frac{1}{2}-p-1} f(\theta) = r^{-\frac{1}{2}-p} f(\theta) \tag{2.6}$$

Again, coming back to the quantity in square brackets from Equation (2.4), we need to find a bound on $\left[\|u\|^2_{H^{p+1}(\Omega^*_e)}\right]$. Now, we know that,

$$\|u\|_{H^k(\Omega)} = \left[\int_\Omega \sum_{\alpha=0}^{k} \left(\frac{d^\alpha u}{dx^\alpha}\right)^2 dx\right]^{\frac{1}{2}} < \infty \tag{2.7}$$

If the highest order derivative of order 'k' in Equation (2.7) above is bounded, then all the other lower order derivatives will be bounded.

Consider the term in square brackets from Equation (2.4),

$$\|u\|^2_{H^{p+1}(\Omega^*_e)} = C\left[\int_{\Omega^*_e} \left(\frac{\partial^{p+1} u}{dx^{p+1}}\right)^2 dx\right] = C\left[\int_0^{2\pi}\int_d^{d+h} f(\theta)\left(\frac{\partial^{p+1} u}{\partial r^{p+1}}\right)^2 r dr d\theta\right] \tag{2.8}$$

Here, the constant 'C' takes care of bound on all the lower order derivatives.

Using equations (2.6) and (2.8), we get,

$$\|u\|^2_{H^{p+1}(\Omega^*_e)} = C\left[\int_d^{d+h} r^{-2\left(p+\frac{1}{2}\right)+1} dr\right]$$

(as all the θ dependence can be clubbed into an unknown constant C)

or,

$$\|u\|^2_{H^{p+1}(\Omega^*_e)} = C\left[\int_d^{d+h} r^{-2p} dr\right] \tag{2.9}$$

From Mean Value Theorem for integrals, we know that,

$$\int_a^b f(x)dx \leq f(x')(b-a)$$

where x' is the point in domain, $x \in [a,b]$, at which the function $f(x)$ attains a maximum value $f(x')$ for all $x \in [a,b]$.

In this case, the function $\left(r^{-2p}\right)$ attains a maximum value at $r = d$.

Therefore,

$$\|u\|^2_{H^{p+1}(\Omega^*_e)} = C\left[\int_d^{d+h} r^{-2p} dr\right] \leq Cd^{-2p}h \tag{2.10}$$

The very purpose of obtaining the optimal convergence rate will be solved if the quantity on right-hand-side of Equation (2.10) is bounded by a constant, i.e.

$$\begin{aligned} & d^{-2p}h \leq C \\ \Rightarrow \quad & Cd^{2p} \geq h \\ \Rightarrow \quad & d \geq C(h)^{\frac{1}{2p}} \end{aligned} \tag{2.11}$$

(Note: This relation holds good for both *two* and *three-dimensional* problems.)

2.3 Model Problem: Edge-Crack Panel

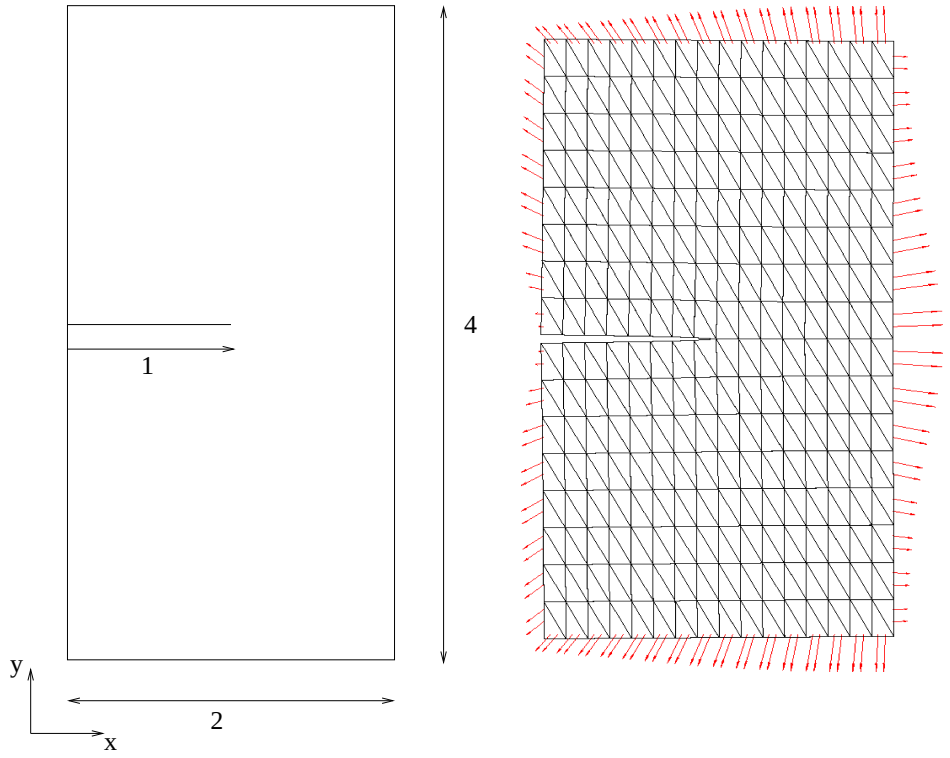

Figure 2.4: *Model problem with a through-the-thickness crack*

The Finite Element simulations in the following study are performed using the Illinois Scientific and Engineering Toolkit *(ISET)*, which is a numeric implementation of the Generalized Finite Element Method. ISET is an in-house research code written in C++ programming language, currently under development by our research group under the supervision and guidance of its creator, Professor C. Armando Duarte from the Department of Civil and Environmental Engineering at the University of Illinois at Urbana-Champaign.

The numerical studies in this project are performed on a 3-D linear elastic fracture mechanics problem as described below. It is an edge-crack panel with uniform thickness of 0.25” throughout and geometric dimensions as shown in Figure 2.4. The problem has a single through-the-thickness crack and is discretized with a uniform mesh of tetrahedral elements. The boundary conditions are applied in the form of exact tractions derived from the first order term of the asymptotic expansion of the Mode I opening of the crack (as shown in Figure 2.4). The value of Young’s Modulus is taken equal to unity. A Poissons ratio value of 0.0 is chosen because in that case it becomes a 2-D problem for which we know the exact solution in the entire domain of the problem and also only one layer of element has been provided in the z-direction. The exact solution helps us in evaluating the exact strain energy of the problem (which is used in this study for calculating the errors), and most importantly, exact boundary conditions can be used at the boundary of

the local problem, so we can make sure that the effect of inexact boundary conditions does not affect this study. The crack has been modeled explicitly by using double nodes at the location of crack surface.

The sequence of meshes used here for the purpose of studying the convergence behavior consists of four meshes, as shown in Figure 2.5, which have been subsequently refined to go from one to another and have been chosen in such a manner that if there is no singularity in the problem, this sequence of meshes would yield an optimal rate of convergence for uniform mesh refinement with repect to the size of the coarse scale global elements. The meshes are created by first generating the uniform mesh of hexahedral elements and then dividing each element into 6 tetrahedral elements.

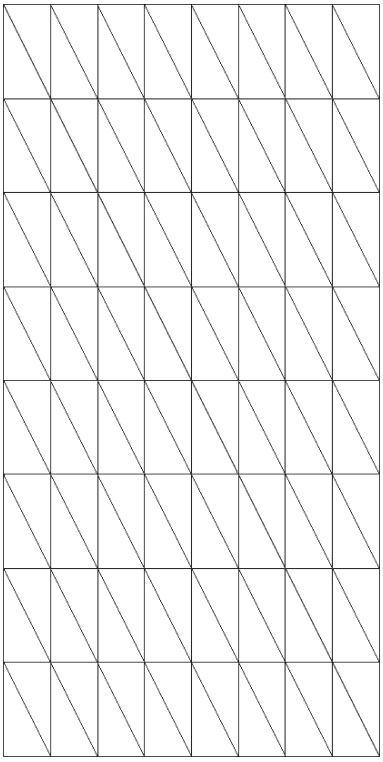

(a) Mesh 1

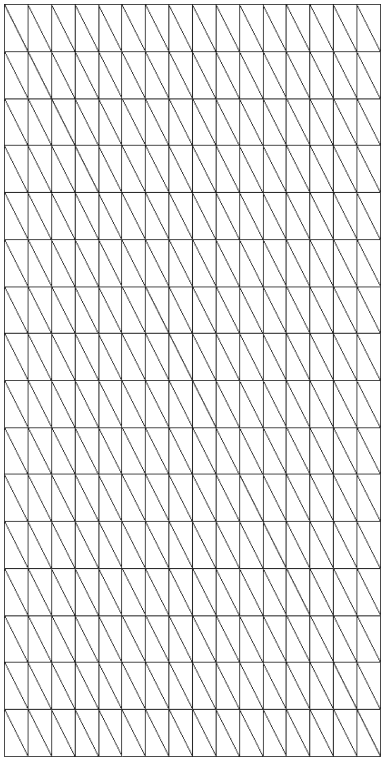

(b) Mesh 2

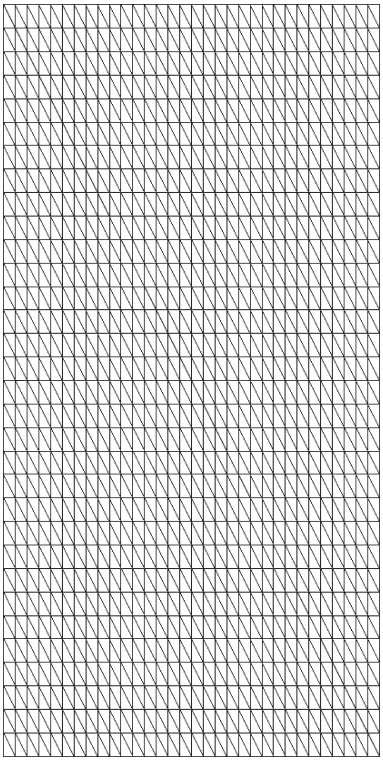

(c) Mesh 3

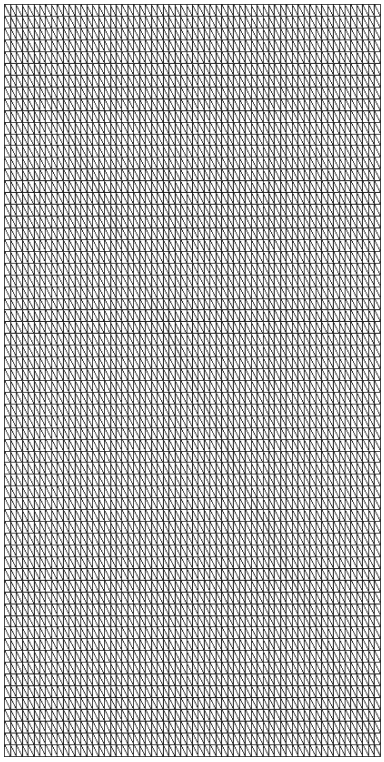

(d) Mesh 4

Figure 2.5: *Initial meshes used for the study*

2.4 Optimal Local Problem Refinement

Firstly, the convergence plots, corresponding to the four meshes shown in Figure 2.5 are presented with respect to the size of the elements in the local problem.

To start with, the geometric domain of the local problem is being defined with the help of a square bounding box of dimensions *1" X 1"* surrounding the crack front, as shown in Figure 2.6, wherein the local mesh was refined uniformly by one level ($nref_{uniform} = 1$) and in a geometric progression towards the crack front by six levels ($nref_{front} = 6$), so as to capture the singularity better at the crack front. A local discretization with one level of mesh refinement around a crack front is taken care of by first bisecting, in the initial mesh, all elements with nodes on the crack front and then bisecting additional elements in order to recover a conforming discretization. The refinement edges of the elements are selected based on the marked-edge algorithm [1, 4]. So, to achieve a refinement level of *nref = n*, this procedure is repeated *n* times. The initial mesh extracted from the global mesh corresponds to the *nref = 0*. This local mesh refinement algorithm also preserves the nesting of local elements into the global mesh, which greatly facilitates the computational implementation. Though, in a general case, the boundary conditions for the local problem would be picked from the FEM solution of the intial global problem, but in this case, exact boundary conditions have been imposed on the boundary of the local problem in the form of Cauchy or Spring Boundary Conditions. Also, in this section, *geometrical enrichment* has been used and the size of enrichment zone in the global mesh is same as the local problem domain.

The notation used in this study is as follows: '*H*'denotes the smallest x-direction dimension of the tetrahedral elements in the global mesh; '*h*' denotes the x-direction dimension of the smallest tetrahedral element (which would be the set of elements next to the crack front) in the local mesh and from now on these dimensions would simply be referred as the size of the elements in the corresponding meshes.

Figure 2.7 shows the Relative error in Energy Norm, computed from the enriched global solution, plotted against the inverse of the size of the element in the local mesh for Mesh 1 (Size of element = H_1) and the different points on the curve correspond to the different levels of crack front refinement in the local mesh. To provide an idea about the size of problem, the number of DOFs in the intial global mesh and local problem without any additional refinement are (*2,040*) and (*1,800*) respectively, whereas number of DOFs in the enriched global problem is (*2,064*), which is *24* DOFs more than in the initial global mesh (corresponding to *3* DOFs per node on each of the *8* enriched nodes of the global problem). For the same mesh, the number of DOFs in the local problem becomes (*66,660*), when we provide a refinement scheme with *1* level of uniform refinement ($nref_{uniform} = 1$) and *6* levels of crack front refinement ($nref_{front} = 6$), whereas the number of DOFs in the enriched global mesh remains the same. The second curve in the plot shows the results obtained with *hp-GFEM* applied on the meshes with same refinement levels as that in $GFEM^{g\text{-}l}$. Here, the *hp-GFEM* is equivalent to the standard finite element method with strongly graded meshes. In the context of

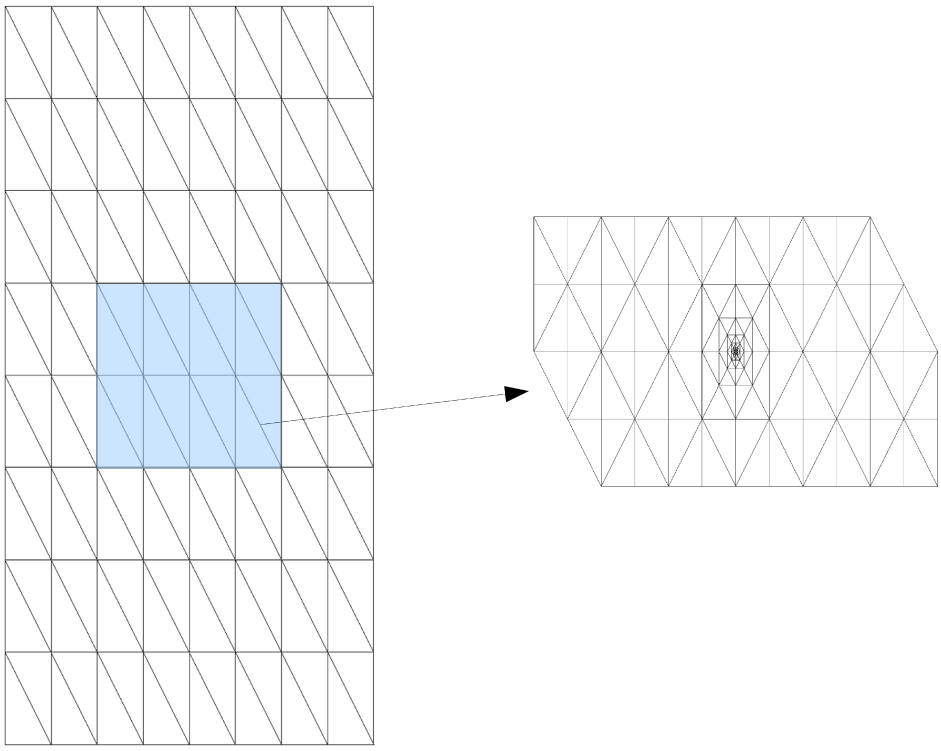

Figure 2.6: *Figure showing the extraction of a localized geometric domain from global mesh to obtain the local mesh*

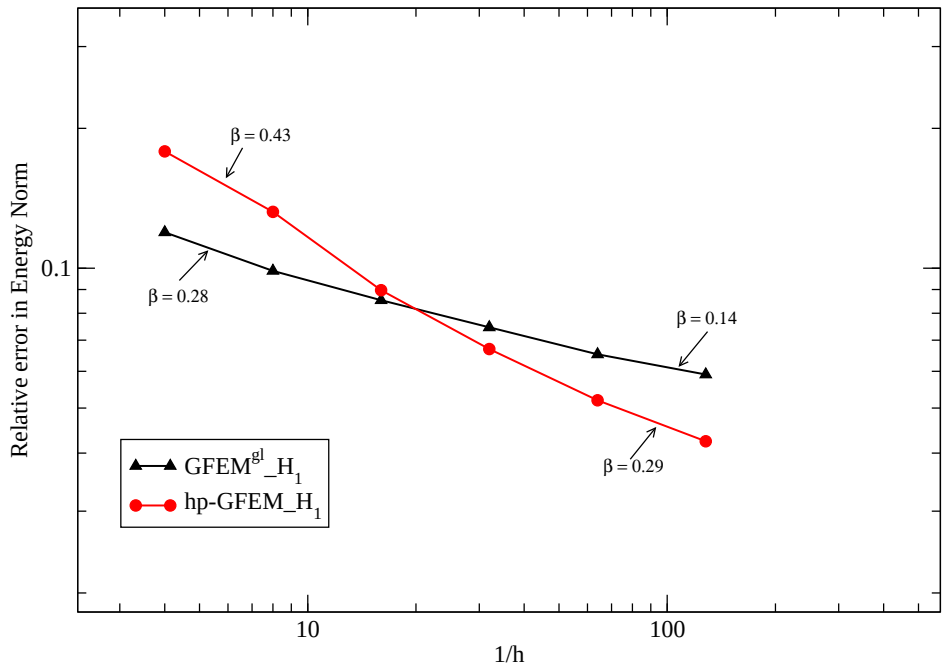

Figure 2.7: *Convergence behavior of the global problem plotted with respect to the local element size for Mesh 1*

the problem at hand, in *hp-GFEM*, the isolation of singularity is attempted by using a highly graded and refined mesh in a localized region. As can be seen from the plot, both the curves show a similar behavior and the convergence rate decreases as we go for higher crack front refinement levels, which indicates that due to a very coarse global mesh, the error away from the crack front starts coming into the picture, as we take care of the error due to singularity, by the crack front refinement. Figure 2.8 shows the results of similar runs performed on Mesh 2 (H_2). As can be seen from

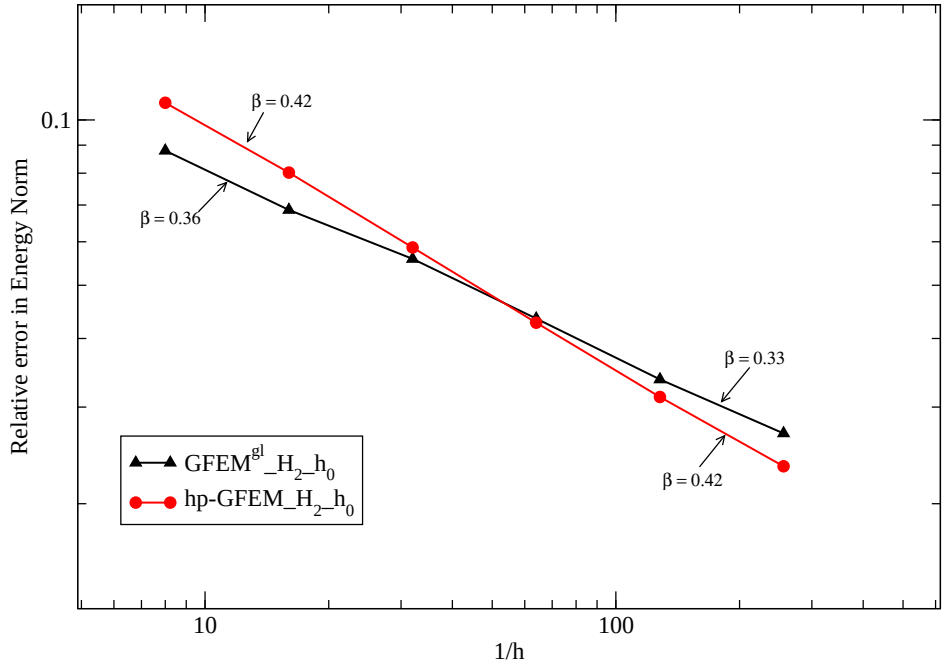

Figure 2.8: *Convergence behavior plotted with respect to the local element size for Mesh 2 ($nref_{uniform} = 0$)*

the plot, there is not much significant reduction in the convergence rate with the refinement levels, and also the two methods (i.e. *hp-GFEM* and *GFEM*$^{g\text{-}l}$) again show a similar behavior. In this plot, the notation h_0 implies no subsequent uniform refinement ($nref_{uniform} = 0$) in the local mesh and is same as the initial mesh extracted from the global mesh. Figure 2.9 shows the results corresponding to the case with $nref_{uniform} = 1$ in the local mesh and thereby halving the element sizes in the local problem mesh. One can notice from this plot that there is a very significant reduction in the convergence rate with subsequently higher crack front refinement levels which can be explained on the basis that although the error levels got reduced locally (in the region of the local problem), because of the refinement, the global error, (i.e. away from the crack front) still remains the same, leading to poor convergence rate.

Therefore, for all the following convergence studies, only crack front refinement and no subsequent uniform refinement ($nref_{uniform} = 0$) has been applied in the local problem. Also, the strategy of using crack front refinement only, in the local problem, turns out to be computationally more efficient and leads to much fewer Number of DOFs for a given error level.

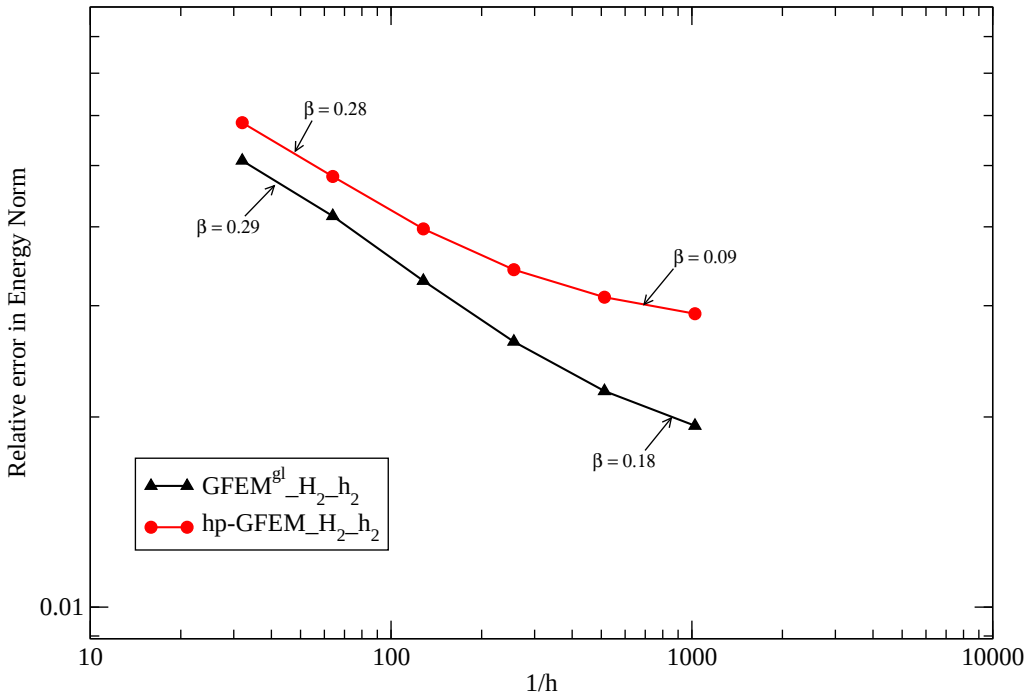

Figure 2.9: *Convergence behavior plotted with respect to the local element size for Mesh 2 ($nref_{uniform} = 1$)*

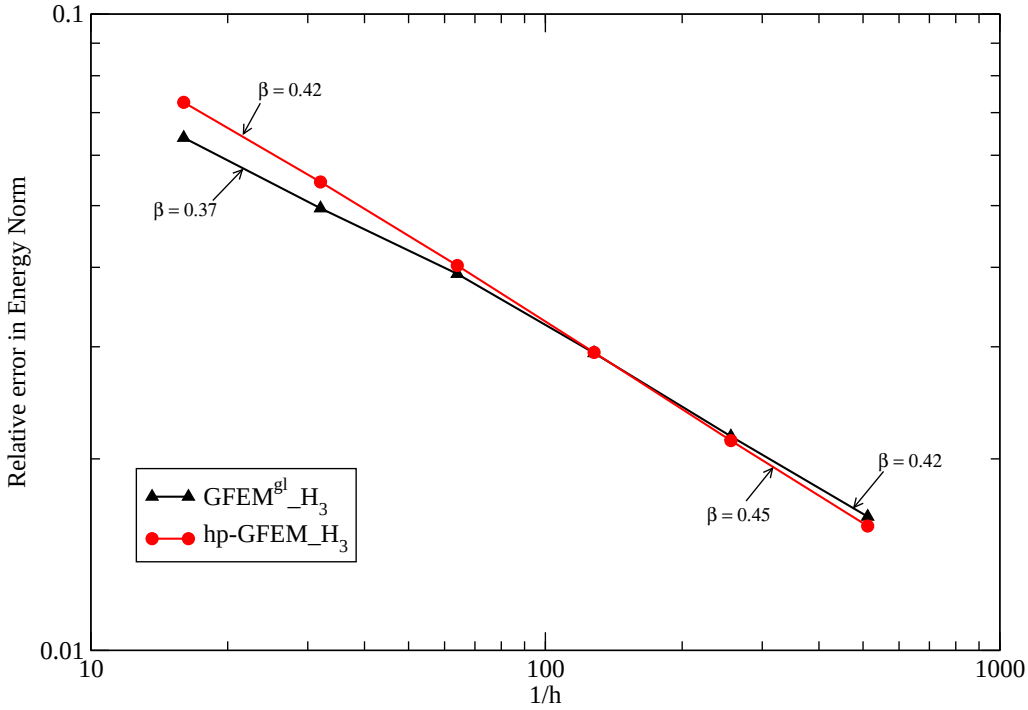

Figure 2.10: *Convergence behavior plotted with respect to the local element size for Mesh 3*

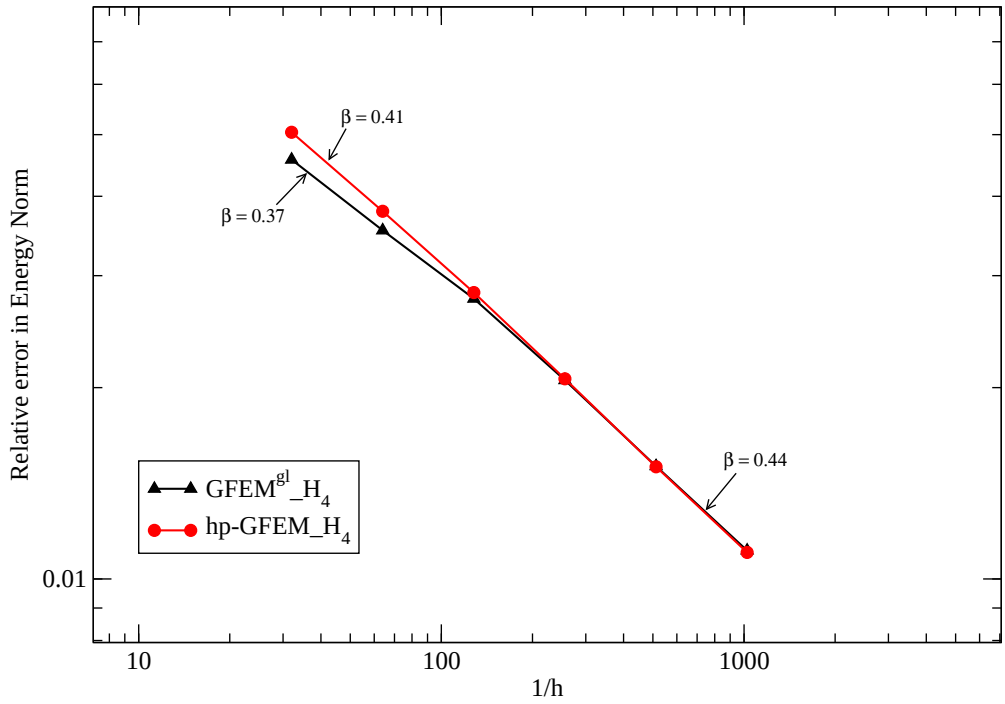

Figure 2.11: *Convergence behavior plotted with respect to the local element size for Mesh 4*

Figures 2.10 and 2.11 show the convergence behavior for Mesh 3 and Mesh 4 respectively, and it can be seen from the plots that the convergence rates have improved quiet a lot in comparison to the previous two coarser global meshes and also the convergence rate does not get any slower or rather its increasing with subsequent crack front refinement levels. *Mesh 4* is the finest mesh used in this study, and with no additional refinement in the local problem, the Number of DOFS in the initial global problem, local problem and enriched global problem are (*102,168*), (*69,000*) and (*105,048*) respectively. In the case of $nref_{uniform} = 1$ and $nref_{front} = 6$, the Number of DOFs in local problem becomes (*288,420*), with number of DOFs in the global problem remaining the same.

Figure 2.12 shows the results from all the four meshes, discussed above, combined together at one place. This clearly shows how the convergence rates improve as a finer global mesh is used and no reduction in convergence rate is observed in case of finer meshes as when compared to with the case of first two meshes.

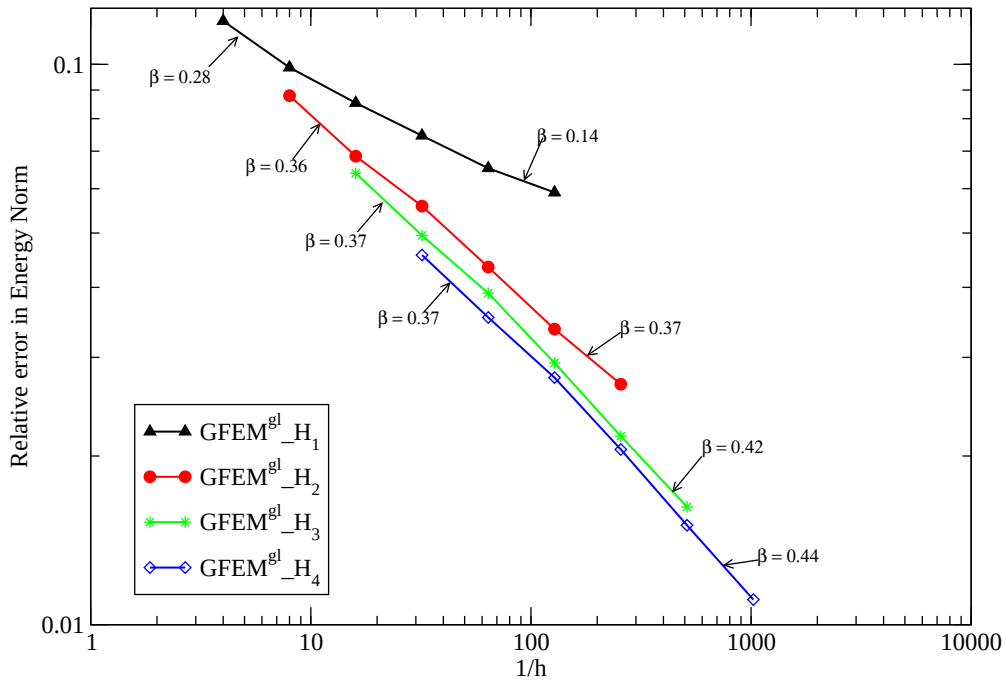

Figure 2.12: *Convergence behavior plotted with respect to the local element size for all the four meshes*

2.5 Effect of Enrichment Zone Size

The model problem and the initial meshes used in this study are same as in the Section 2.4. However, the size of the local problem has been increased to 2" in the y-direction. For different simulation cases, the domain of the local problem is being kept the same (*1.5" X 2.0"*, shown as blue rectangular box in the Figure 2.13), and the domain of the enrichment zone is being varied as shown by different colored rectangular boxes. The local domain has been chosen to be same implying exactly the same local solution in each case, so that we can study the effect of varying only the size of enrichment zone. The first enrichment zone is the same as the entire local problem shown as a blue rectangular box, and in this case all the nodes of the global problem lying within the region of the local domain will be enriched with the solution of the local problem. The second one is of the size *1.0" X 2.0"* (shown in orange), third enrichment zone is shown as a green rectangular box (*0.5" X 2.0"*), and the small red square corresponds to the case of topological enrichment in which only the nodes lying along the crack front are enriched. Thus, in all the cases of geometrical enrichment, the size of the enrichment zone in y-direction is being kept same as 2" and is varied linearly in the x-direction.

The sequence of meshes used to study the convergence is shown in figures 2.14 and 2.15. In the figures, the picture on the left hand side shows the initial global mesh with the region of local problem marked in blue rectangular box. The picture in the centre shows the local problem which is pulled out of the initial global mesh and then a certain refinement scheme with 8 levels of crack front refinement ($nref_{front} = 8$) has been performed on this local problem. The polynomial order of the elements in the local problem has been taken equal to *4*, so as to capture the local solution very accurately. And for the coarse scale mesh, elements of order *2* have been used, so the optimal rate of convergence in energy norm with respect to the coarse scale element size is *2*.

The picture on the right hand side of the figures shows the coarse scale global mesh enriched with the local solution (Enriched Global Mesh), and the red nodes are the ones which correspond to the global-space clouds enriched with global-local enrichment functions. Also, it can be seen from these figures that as the global mesh is refined, more and more enrichment DOFs are added in the enriched global problem which adds to the computational cost. Further, note that these figures correspond to the case of enrichment box of size *1.5" X 2.0"*.

For Fracture Mechanics problems, where the singularity of the problem affects the convergence behavior, the rate of convergence in the energy norm is governed by the order of the Hilbert space, $'k'$ (i.e. by the term *(k-1)* in Equation (2.1)), in which the analytical solution of the problem lies. And for the model problem at hand, $k = \frac{3}{2}$, and therefore, if the singularity prevails, then the theoritical convergence rate for this problem with uniform *h-refinement* would be $\frac{1}{2}$. Now, the goal is to achieve the optimal convergence rate, i.e. the one governed by the term $'p'$ (polynomial order of the elements), given in Equation (2.1), which is being tried to achieve by using the global-local enrichment functions in a geometric region big enough to isolate the singularity of the problem.

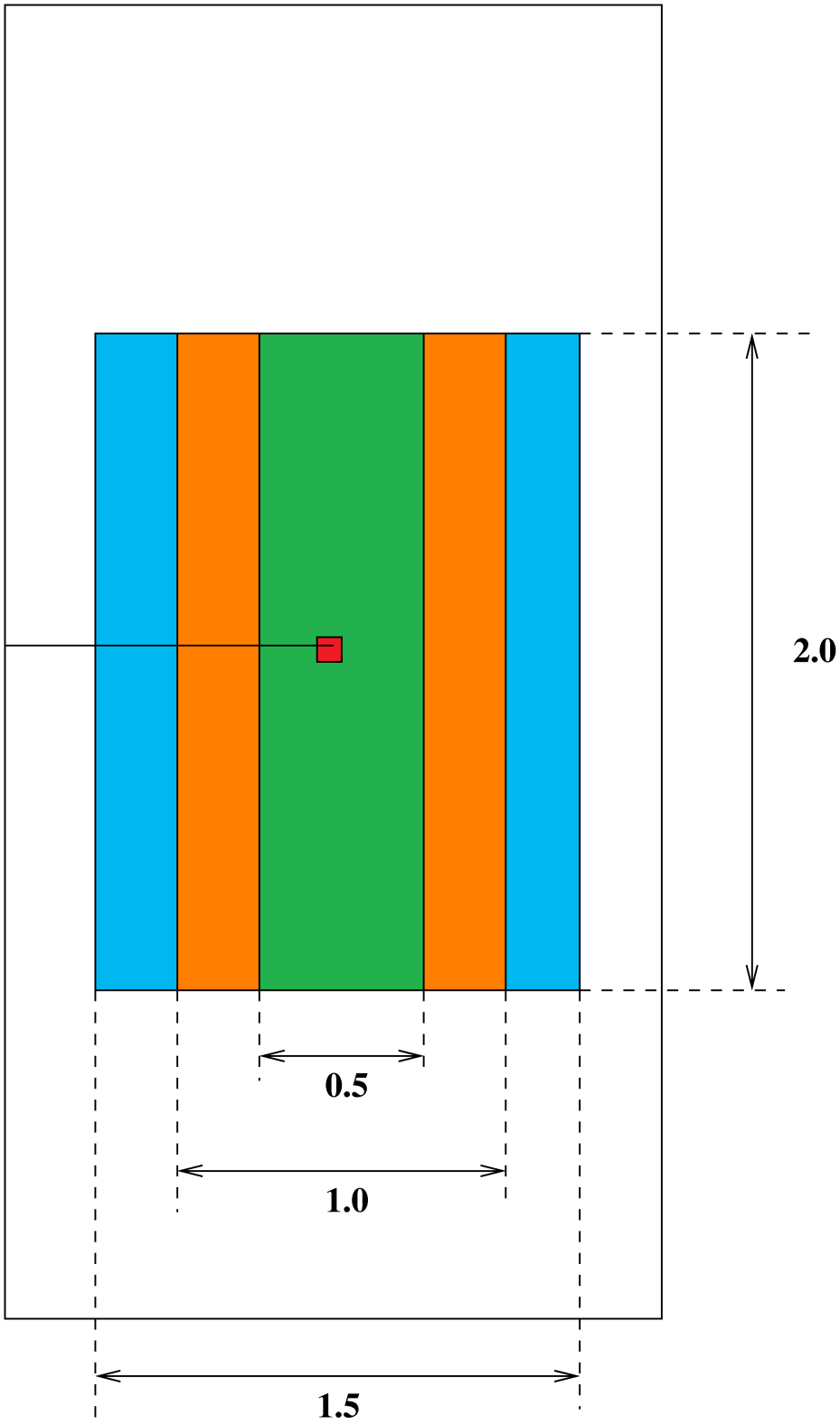

Figure 2.13: *Figure showing different enrichment zones and local problem*

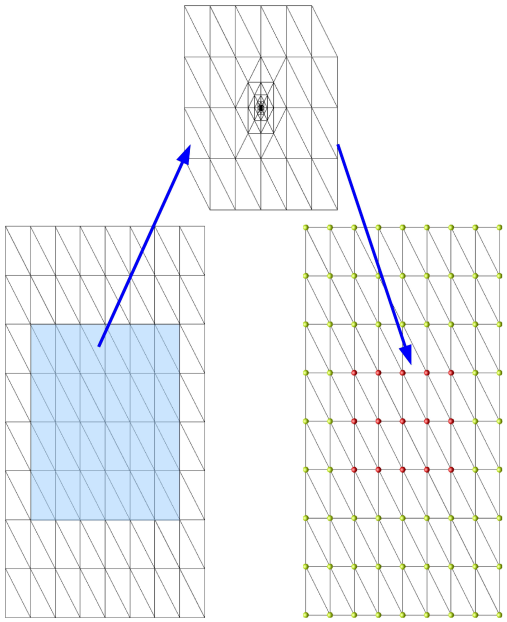

(a) Mesh 1

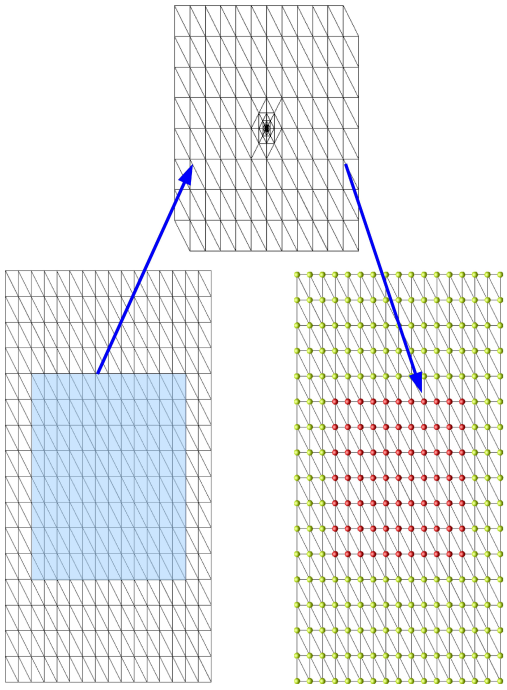

(b) Mesh 2

Figure 2.14: *Figures showing Mesh 1 and 2 from the sequence of meshes used in the study: left hand side picture shows the initial global mesh with the region of local problem marked in blue rectangular box, picture in the center shows the local problem mesh and the picture on the right shows the enriched global mesh and the nodes marked in red are the ones enriched with the local solution.*

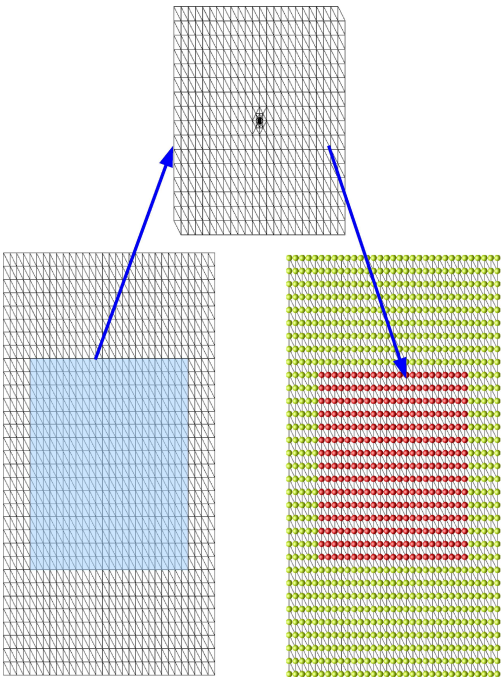

(a) Mesh 3

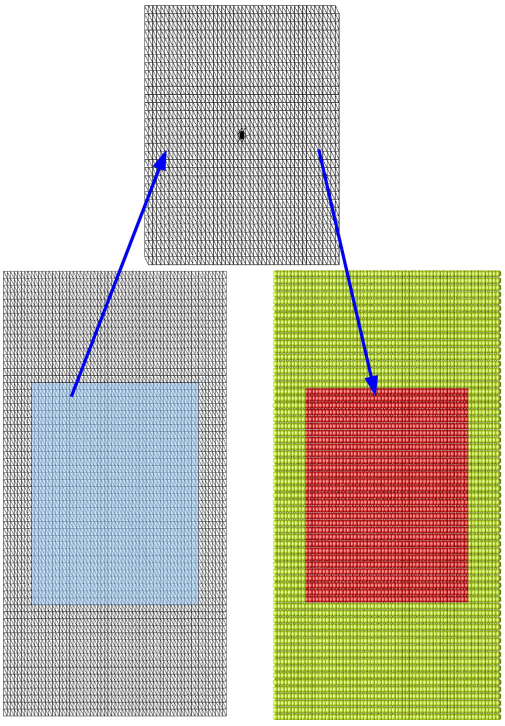

(b) Mesh 4

Figure 2.15: *Figures showing Mesh 3 and 4 from the sequence of meshes used in the study: left hand side picture shows the initial global mesh with the region of local problem marked in blue rectangular box, picture in the center shows the local problem mesh and the picture on the right shows the enriched global mesh and the nodes marked in red are the ones enriched with the local solution.*

Figure 2.16 shows the plots corresponding to different simulations which were run on the sequence of meshes shown in figures 2.14 and 2.15. The first curve corresponds to the case of the standard Finite Element Method with uniform $H-refinement$, wherein the simulations were run only on the initial global meshes without any enrichment or a subsequent step. It gives a convergence rate close to 0.5 and that is expected too in this problem as discussed above.

As can be seen from the red curve, that although the error levels are much lower in case of topological enrichment when compared with the case of standard FEM, because of a much lower value of constant C in the Error Equation (2.1), the convergence rate is still very poor and is equal to *0.5*, which means that it is not being able to isolate the singularity and is giving us the convergence rate corresponding to the problem in which the singularity governs the convergence rate, so as $H \rightarrow 0$ with the mesh refinement, the enrichment area also tends to *0* and thereby not capturing singularity adequately, resulting in this poor convergence behavior.

Now, it can be clearly seen from these plots, that the geometrical enrichment improves the convergence rate drasti-

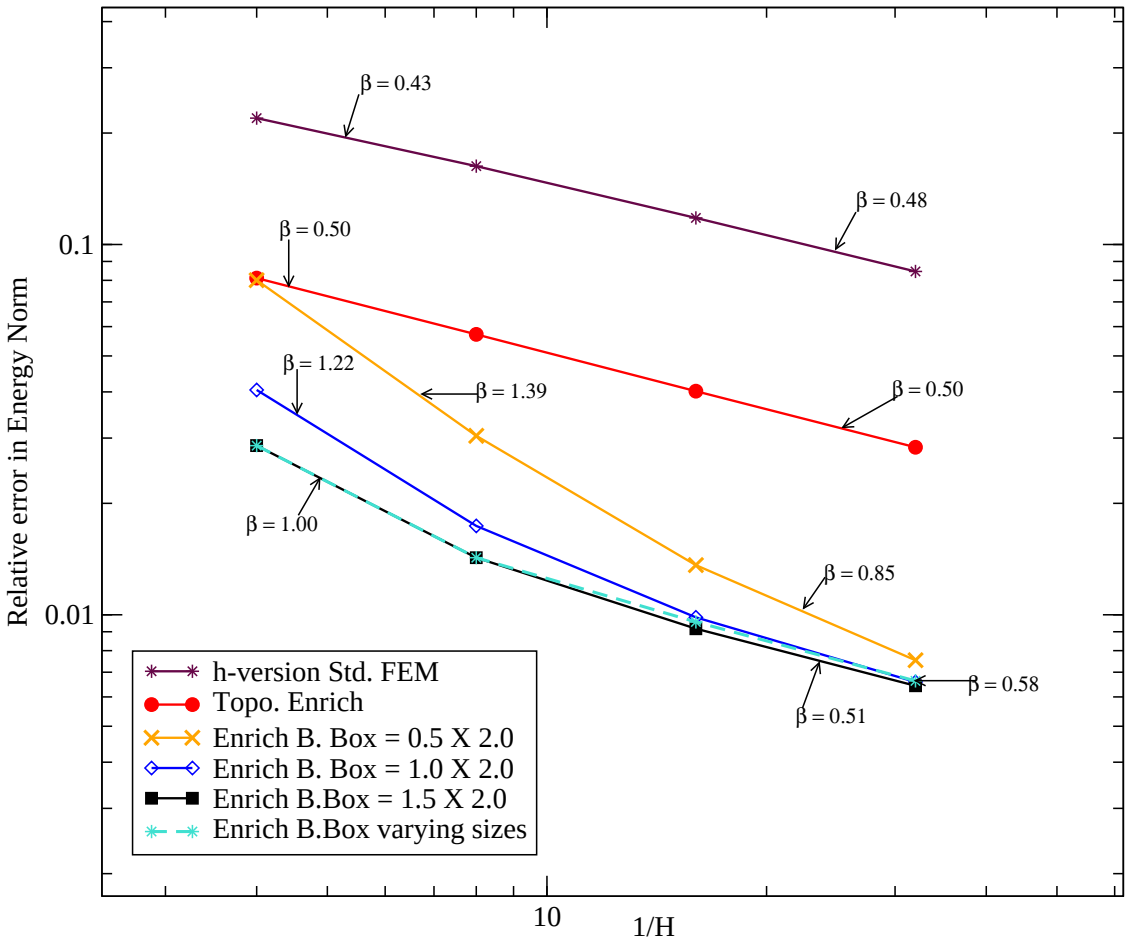

Figure 2.16: *Convergence plots showing* GFEM$^{g\text{-}l}$ *results: Relative error in Energy Norm plotted against the inverse of the global element size, H, for different enrichment zone sizes.*

cally and we see very high convergence rates in all the other cases plotted in Figure 2.16. Further, it can be seen from the above curves that the convergence gets slower as we move along the curve. That is, the effect of the singularity in the local problem starts dominating and it indicates that for finer levels of refinement in the global mesh, more refinement is needed in the local mesh to achieve the same convergence behavior as observed in the initial part of the curves.

Though, it can be noticed that the convergence rate is still not optimal (i.e. not equal to $p = 2$), it is, however, significantly close to the optimal convergence rate and the reason for that is explained by the fact that there are computational limitations on how much the local mesh can be refined. The more refined the local mesh is or in other words, the more accurate the local solution is, the better the singularity gets isolated, and as a result we get better convergence rates and this can be studied by varying only the quality of the local solutions, keeping the global parameters (global mesh discretization, size of enrichment zone etc.) the same and adjudging its effect on the convergence behavior in the global problem . This point is further reinforced by the results in figures 2.17, 2.18 and 2.19. Figure 2.17 shows the effect of changing the quality of local solution, by using different levels of crack front refinement ($nref_{front} = 4,6,8$) in the local problem, on the convergence behavior in the global problem (the curve with the solid line is same as the black curve in Figure 2.16). The Number of DOFs in the local problems for *Mesh 1* corresponding to $nref_{front} = 4,6,8$ are (*12,180*), (*36,300*) and (*129,540*) respectively, whereas the Number of DOFs in the enriched global problem is (*2,142*) . This figure clearly shows that as the local problem is refined more, or in other words, if the local solution is captured more accurately, the convergence rate in the enriched global problem improves.
Another possibility is to use meshes in which the size of the elements decreases faster towards the singularity than in the way it is being done here (reducing by half every subsequent layer of elements) [27].

Figure 2.18 shows the effect of using branch-function enrichments in the entire local domain. The branch-function enrichments are nothing but the enrichment functions generated from our knowledge of the exact solution (asymptotic expansion of the Mode I opening of the crack) near the crack front. It can be seen that with the use of branch-function enrichments, the convergence rates improve drastically and become very close to the optimal convergence rate, which again reinforces the fact that if the local solution is captured accurately, convergence behavior of the enriched global problem gets much better. Also, even in the case of these branch-function enrichments, topological enrichment still gives a poor convergence rate of *0.50*, which shows that it doesn't matter how accurately the local solution is captured, the (topological) enrichment won't be effective with respect to convergence rate as $H \rightarrow 0$.

Further, the use of branch-functions only in the local problem will not affect the number of Enrichment Degrees of Freedom in the Enriched Global Problem and that would still remain as *3 DOFs* per node. The Number of DOFs

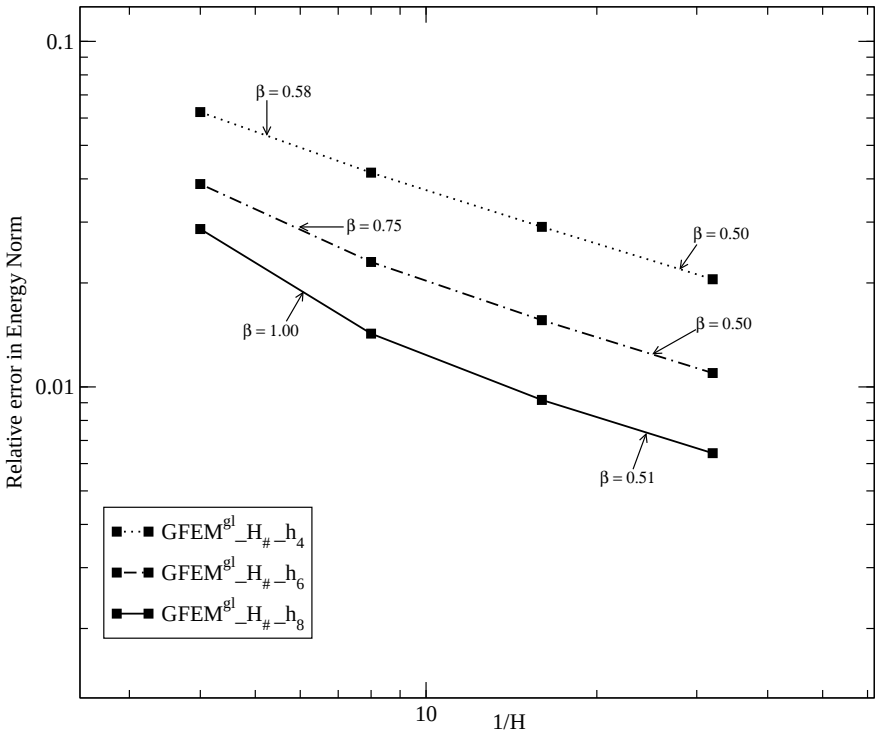

Figure 2.17: *Convergence behavior shown for different levels of crack front refinement ($nref_{front} = 4, 6, 8$) in the local problem corresponding to the case of enrichment zone size of 1.5" X 2.0"*

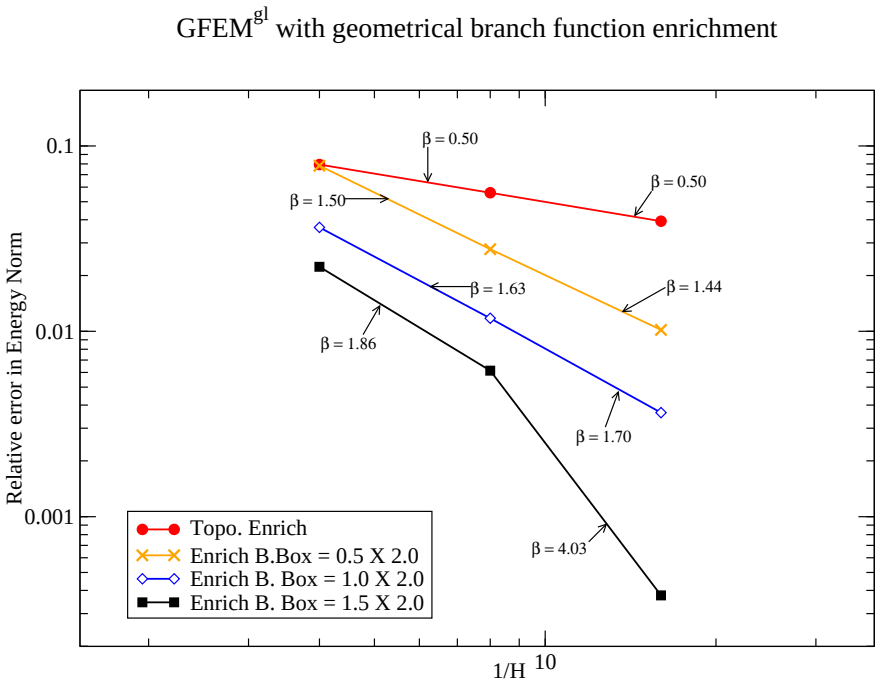

Figure 2.18: *Convergence behavior showing the effect of using branch-function enrichments in the local problem corresponding to the case of enrichment zone size of* 1.5"X2.0"

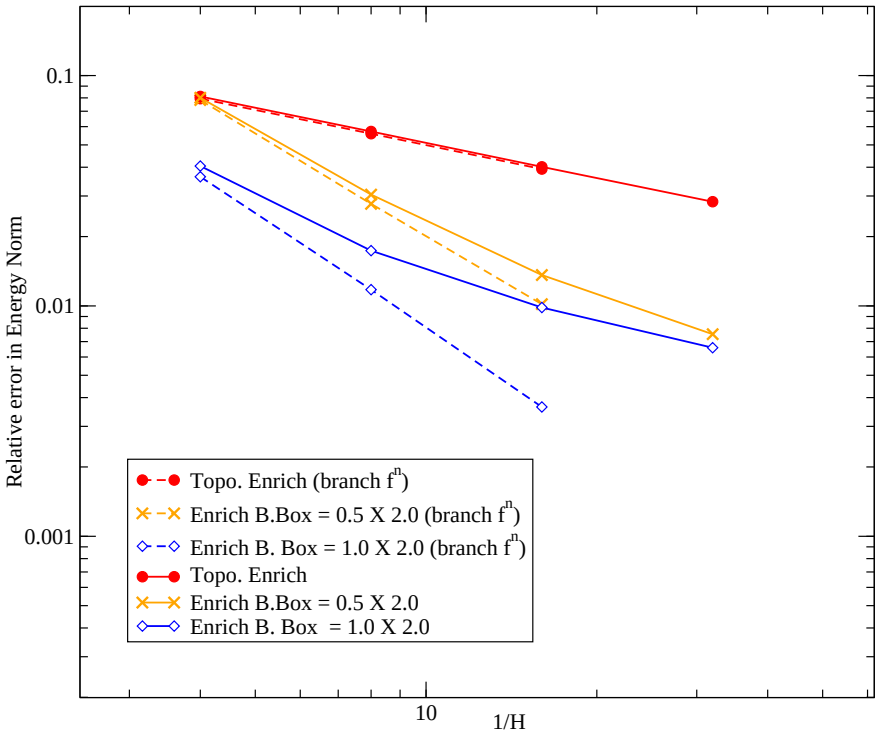

Figure 2.19: *Convergence behavior showing the comparison between the cases with and without branch-function enrichments in the local problem corresponding to the case of enrichment zone size of* 1.5"*X*2.0"

in the local problem with *8* levels of crack front refinement ($nref_{front} = 8$) increases to (*142,266*), because of the branch-function enrichments, whereas, for the enriched global problem, remains the same ($= 2142$). Furthermore, in a practical problem, the local mesh would be a small region near the crack tip (front), wherein the crack can be assumed to be planar, for which the theoritical expression of the elasticity solution is known. Although, there are integration issues associated with these branch function enrichments [21], and therefore a large number of integration points have been used in this study adding to the computational cost, the singularity would be less steeper slightly farther from the crack front in comparison to the region close to the crack front, and thus, the integration errors should not be significant for the elements, slightly away from the crack front.

Figure 2.19 sums up and compares the results from the two cases: with and without the branch-function enrichments in the entire local domain. The dotted curves correspond to the case with branch function enrichments in the local problem (Figure 2.18) and the ones without the branch-function enrichments are shown as solid lines (Figure 2.16). Topological enrichment, yields almost the exact same behavior in the two cases, whereas a clear improvement can be seen in the convergence rates with the use of branch function enrichments as when compared to the case without branch function enrichments. The branch-function enrichments are used in this study, only to show that the convergence rates improve, if the local solution characteristics are captured accurately, because although better results

are obtained by the use of these enrichments, computational complexity increases in terms of dealing with numerical integration issues associated with these enrichments.

Therefore, after all the discussion made above (in reference to figures 2.17, 2.18 and 2.19), it is clear that, this is not any deficiency in the method that the optimal convergence is not obtained, it is just because the local solution is not captured as accurately as required to get the optimal convergence behavior.

Effect of varying enrichment zone size: Now, going back to Figure 2.16, it can be easily seen that going from enrichment zone size of *0.5" X 2.0"* to the one with enrichment zone size of *1.0" X 2.0"*, a lot is gained in terms of the convergence rate and the error levels, but not as much while going from *1.0" X 2.0"* to *1.5" X 2.0"* enrichment zone size, and the curves almost overlap for the later two cases, even though the size of enrichment zone (and hence the number of additional enrichment degrees of freedom) is increasing linearly in the two cases (And one of the reasons to keep the y-dimension of the enrichment zone as constant and only changing the x-dimension was to vary the area of the enrichment zone linearly). This indicates that there exists an optimal enrichment zone size (as was also seen in theoretical analysis given by Equation (2.11)) beyond which it doesn't help much even if the size of the enrichment zone is further increased. For the problem at hand, it seems to be lying between second and third enrichment zone regions (as marked in Figure 2.13). The dotted blue curve in this figure corresponds to the enrichment zone sizes obtained by the theoretical relationship given in Equation (2.11). The first enrichment zone size for the coarsest mesh can be picked up on the basis of the user judgment, so as to obtain close to optimal convergence behavior and in this case it has been taken from the best case at hand, i.e. enrichment zone of size *1.5" X 2.0"*. And as this large enrichment zone size is for the coarsest mesh, so it would not add many DOFs in the enriched global problem. Then, for further refined meshes, i.e. for meshes *2-4*, the enrichment zone sizes have been reduced based on Equation (2.11). For example, Equation (2.11) leads to the enrichment zone size of *0.9" X 2.0"* for mesh *4* when starting from enrichment zone size of *1.5" X 2.0"* for *mesh 1*, which is a very significant reduction in the enrichment zone size given that the error levels corresponding to the two cases for *mesh 4* are not considerably different. Table 2.1 lists the *x-dimension* of the enrichment zone obtained by using Equation (2.11) for all the meshes.

Mesh	*x-dimension* of the enrichment zone
Mesh 1 ($H_1 = 0.25$)	1.5
Mesh 2 ($H_1 = 0.125$)	1.26
Mesh 3 ($H_1 = 0.0625$)	1.06
Mesh 4 ($H_1 = 0.03125$)	0.9

Table 2.1: *Theoretical estimate of sizes of the enrichment zone based on Equation (2.11) for different meshes*

This can help in significantly cutting down the computational cost by reducing the enrichment degrees of freedom, especially in a large complex problem of industrial setting. One more factor which indirectly affects the computational cost is that while evaluating the stiffness matrix component corresponding to the global-local enrichment degrees of freedom, the integration is performed by looping over the local problem elements lying within the corresponding global-local enrichment cloud, so if there is a reduction in the number of nodes (or clouds) having global-local enrichment functions, subsequently would be the reduction in the amount of work involved in looping through the local problem elements (for the purpose of performing integration).

This point (of additional enrichment degrees of freedom) is further made clear by plotting the error levels from Figure 2.16 with respect to the Number of Enrichment degrees of freedom (= Number of DOFs in the Enriched Global Problem - Number of DOFs in the initial global mesh) on the x-axis. The plots in the Figure 2.20 show how much is achieved in terms of error level with addition of the "*Enrichment Degrees of Freedom*". Especially, the last points of the three curves are pretty close with respect to the error levels (i.e. *y-coordinates*) but not so with respect to the number of additional Degrees of Freedom (i.e. *x-coordinates*) which indicates that a smaller enrichment zone size is enough to get similar error levels for a very fine mesh like '*Mesh 4*' in this example. This is also indicated by the Equation (2.11),

$$d \geq C(h)^{\frac{1}{2p}}$$

wherein reducing 'h' would also reduce the size of enrichment zone, not linearly though.

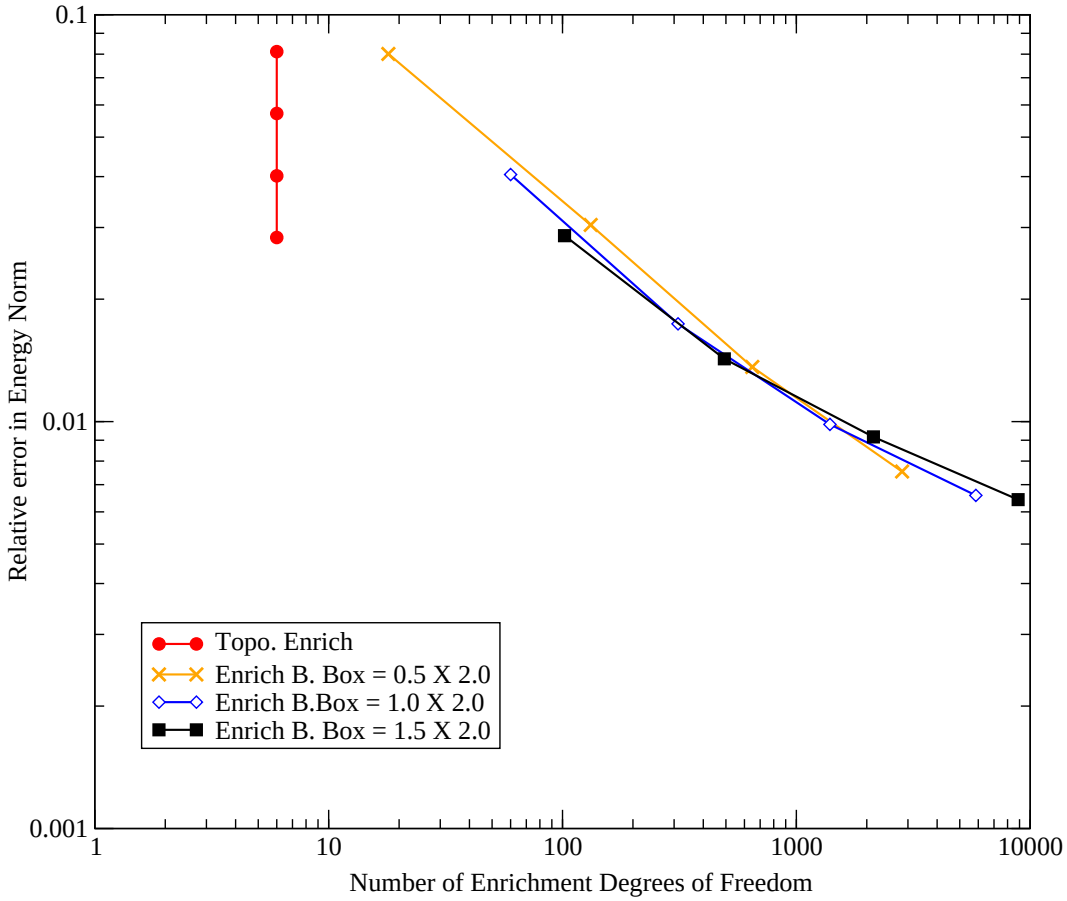

Figure 2.20: *Convergence behavior plotted with respect to the Number of Enrichment Degrees of Freedom (= Number of DOFs in the Enriched Global Problem - Number of DOFs in the initial global mesh).*

Effect of Local Problem Refinement: Now, the effect of refinement in the local problem, on the global behavior for different enrichment zone sizes is investigated here. Figure 2.21 shows the relative error in energy norm of the global problem, plotted against the different enrichment zone sizes for three different levels of crack front refinement ($nref_{front} = 4, 6, 8$) in the local problem. Each dotted vertical line in these plots correspond to different enrichment zone sizes and the three points on these vertical lines correspond to different levels of crack front refinement, $nref_{front} = 4$, $nref_{front} = 6$ and $nref_{front} = 8$ from top to bottom respectively. It can be seen from these plots that the similar behavior is observed for the two meshes (*Mesh 2* and *Mesh 3*) and the results improve quiet a lot coming from the case with $nref_{front} = 4$ to $nref_{front} = 6$, but not as much going from $nref_{front} = 6$ to $nref_{front} = 8$. Also, error levels are quite close in the cases of *Enrich 2* and *Enrich 1*, in comparison to the steeper decrease in the error levels when we go from *Enrich 3* to *Enrich 2* (i.e. the blue section of the curves is steeper than the orange section). An important point to be observed from these plots is that the effect of enrichment zone size (i.e. the reduction in error levels with larger enrichment zone sizes) is less pronounced for *Mesh 3* than in *Mesh 2*, which is in agreement with our estimate of optimal size of enrichment zone, $d \geq C(h)^{\frac{1}{2p}}$ (Equation 2.11), that indicates smaller optimal size of the enrichment zone for a finer mesh (smaller element size ,'h').

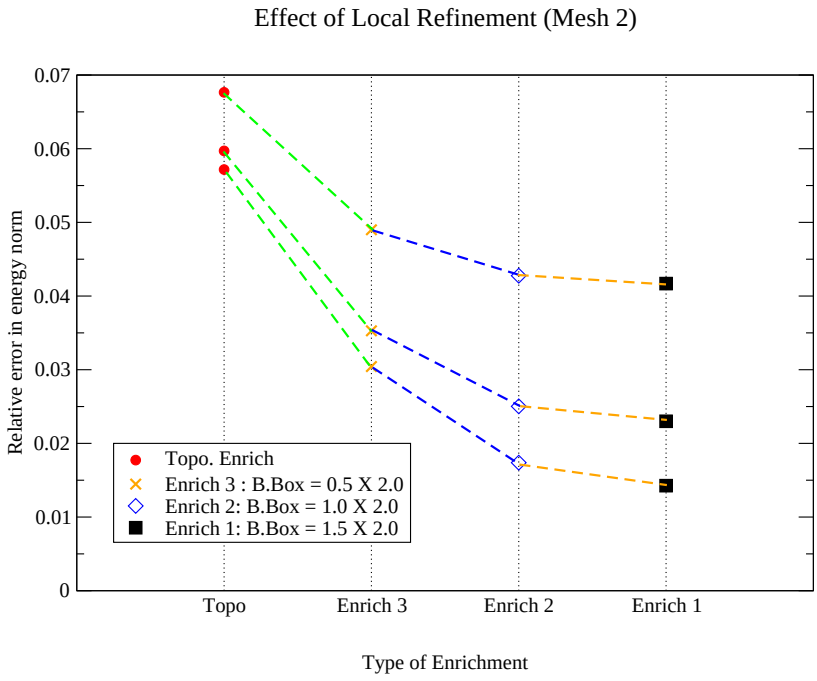

(a) Mesh 2

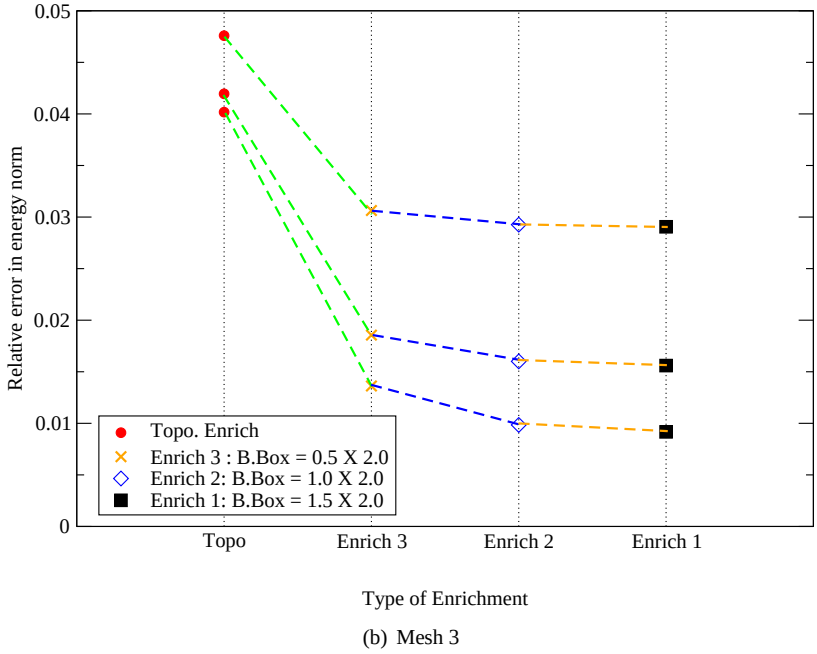

(b) Mesh 3

Figure 2.21: *Figure showing the effect of Local refinement on the Global behavior with different enrichment zone sizes for* (a) *Mesh 2 and* (b) *Mesh 3 for three different levels of crack front refinement in the local problem (*$nref_{front} = 4, 6, 8$*)*

Convergence of Stress Intensity Factor: Until now, the effect of different enrichment zone sizes has been studied with the help of a global quantity: Relative error in strain energy norm. Now, lets see how the enrichment zone size affects a local quantity- Stress Intensity Factor (*SIF*), which is an important quantity of interest from practical standpoint for Fracture Mechanics problems. The *SIFs* have been extracted using the Cut-off Function Method [23] with radii ρ_1 and ρ_2 being chosen based on the numerical experience and making sure that the entire cylindrical domain lies within the enrichment zone region [25]. This allows capturing the solution in terms of local problem enrichments in a better way and hence the outer radius, ρ_2 was taken as 0.20", which lies within the smallest enrichment zone of size *0.5" X 2.0"*. For this problem, the exact value of the *Mode I Stress Intensity Factor* is, $K^I_{exact} = 1.0$ (also, there is no *Mode II* or *Mode III* opening for this problem). Figure 2.22 shows the relative error in Mode I stress intensity factor, plotted against the inverse of the global element size, H for different enrichment zone sizes. Again, the topological enrichment shows higher error levels, whereas the curves corresponding to the geometrical enrichments show much lower error levels. It is known that, theoretically, the SIFs should converge at least as fast as the strain energy [27] and that is what can be seen from the convergence rates marked in these plots. Also, similar to as what was observed in the convergence of strain energy, the results corresponding to the enrichment zone sizes of *1.5" X 2.0"* and *1.0" X 2.0"* are very close to each other and are much better than the ones corresponding to the enrichment zone size of *0.5" X 2.0"* (the second last point on the orange curve, corresponding to the *0.5" X 2.0"* enrichment box seems to be anomalous, and this won't be the case in general).

Comparison with *hp-GFEM*: Now, the behavior of the solution of this problem from *hp-GFEM* is studied, and the results from *GFEM*$^{g\text{-}l}$ are compared with that from the *hp-GFEM*. To keep the two methods on the same ground, equivalent discretizations have been used; the same refinement strategy has been adopted in a localized bounded region in *hp-GFEM* as was used in the local problem in *GFEM*$^{g\text{-}l}$. The sequence of meshes used for this study has been shown in Figure 2.23 for the case with localized refinement zone size of *1.5" X 2.0"* (Mesh *4* has not been shown in this figure due to some graphics problem). The nodes marked in red indicate a high polynomial order of *4* (which is the same as that of the local problem in *GFEM*$^{g\text{-}l}$) associated with the elements which span the space of these clouds (corresponding to the red nodes). Figure 2.24 shows the plots obtained from the *hp-GFEM* simulations being run on the meshes shown in Figure 2.23. As we can see, the results show similar behavior as in case of *GFEM*$^{g\text{-}l}$, and quite a lot is gained while going from local refinement zone of size *0.5" X 2.0"* to *1.0" X 2.0"*, but not as much going further and the later curves almost overlap each other. Again, the error levels and the convergence rates are much better in the case of *hp-GFEM* as when compared to the standard *FEM* (i.e. with uniform *H-refinement*), results of which are also shown in the same figure, therefore proving the effectiveness of providing high polynomial order and very fine mesh in a localized region close to the singularity.

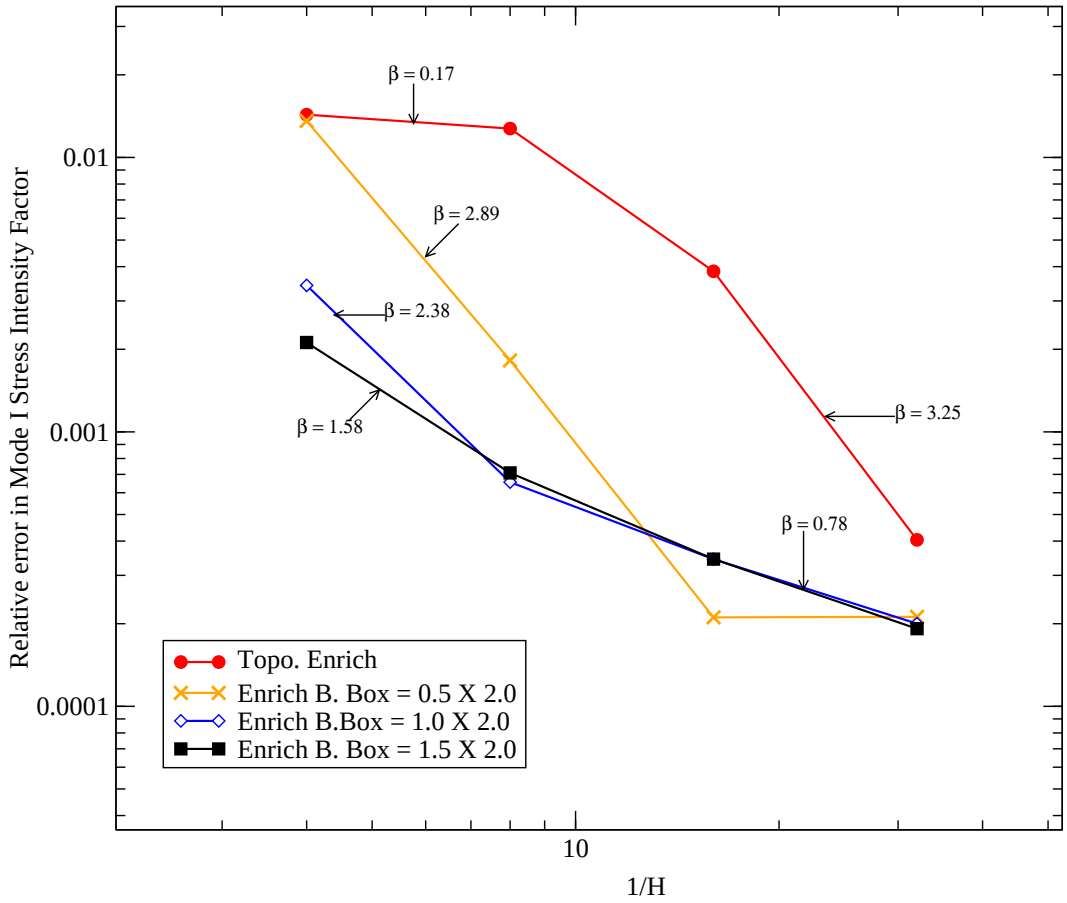

Figure 2.22: *Figure showing Relative error in Mode I Stress Intensity Factors (SIF), plotted against the inverse of global element size, H, for different enrichment zone sizes.*

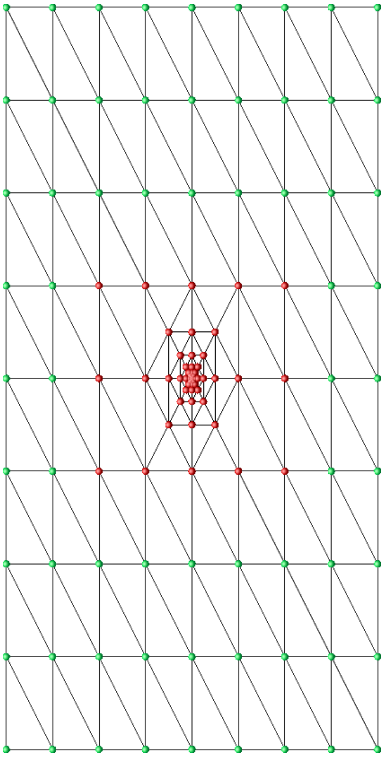

(a) Mesh 1

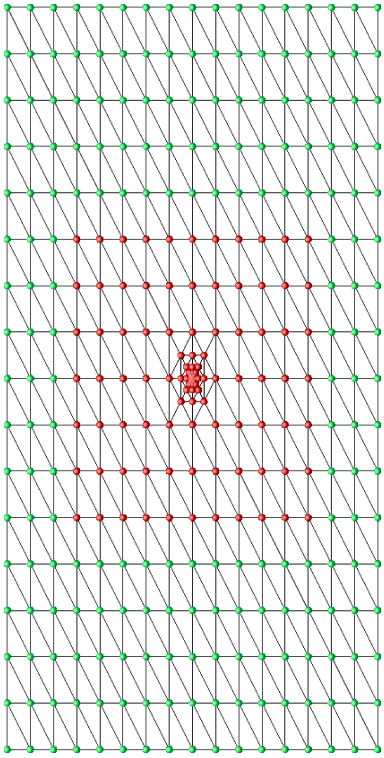

(b) Mesh 2

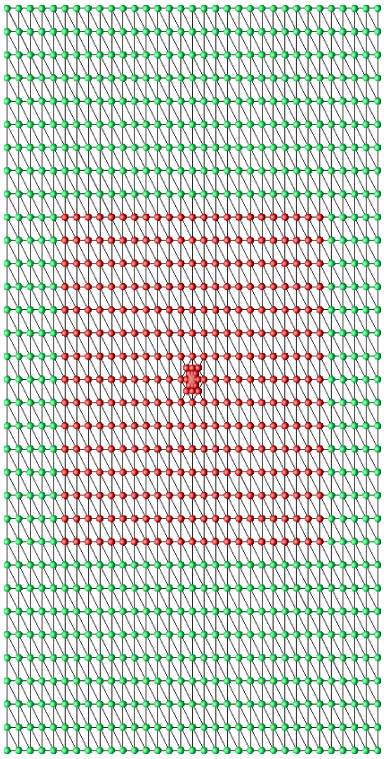

(c) Mesh 3

Figure 2.23: *Meshes used for studying results from hp-*GFEM

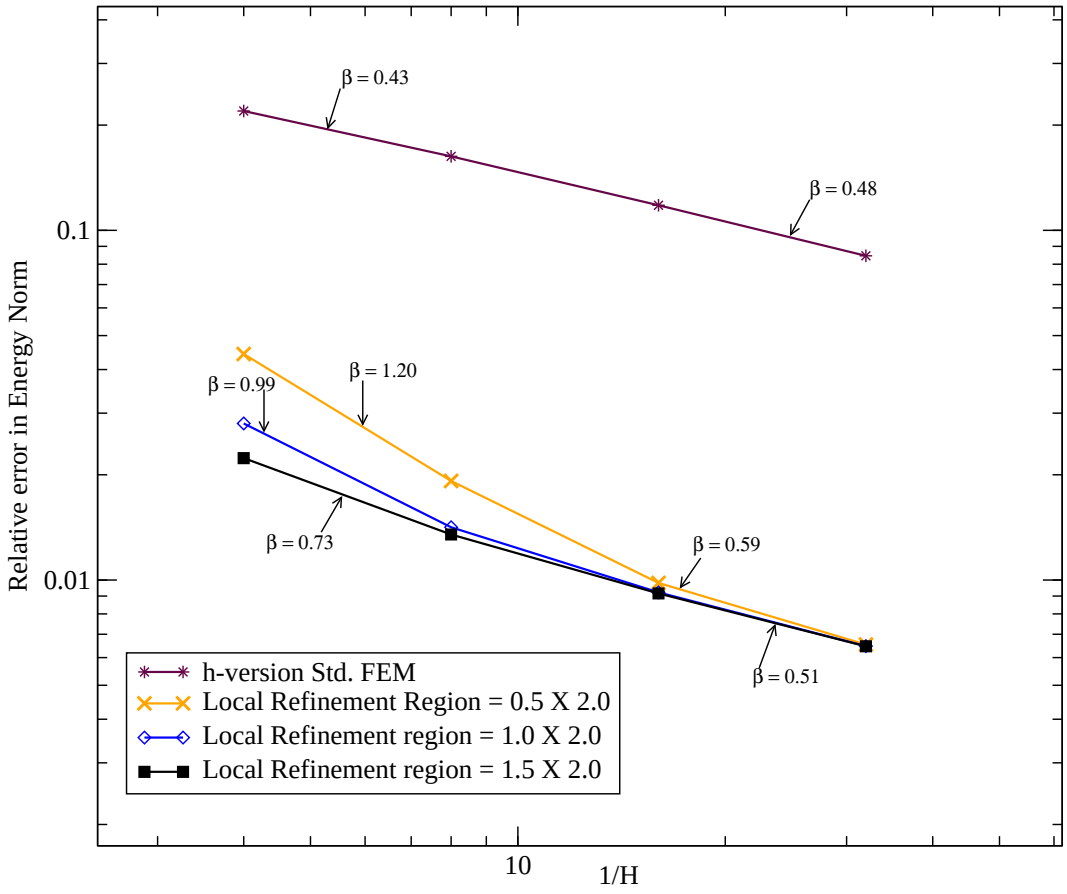

Figure 2.24: *Convergence plots showing hp-*GFEM *results: Relative error in Energy Norm plotted against the inverse of the global element size, H, for different enrichment zone sizes.*

Figure 2.25 shows how the two methods compare with each other for the same localized refinement region (or enrichment zone) size. Though, it can be clearly seen here that *hp-GFEM* is giving lower error levels than *GFEM*$^{g\text{-}l}$, but that might not be true in general and is very problem dependent. The main point is that both the methods behave in a similar way and the role of local refinement region in *hp-GFEM* is similar to the role of enrichment region in *GFEM*$^{g\text{-}l}$.

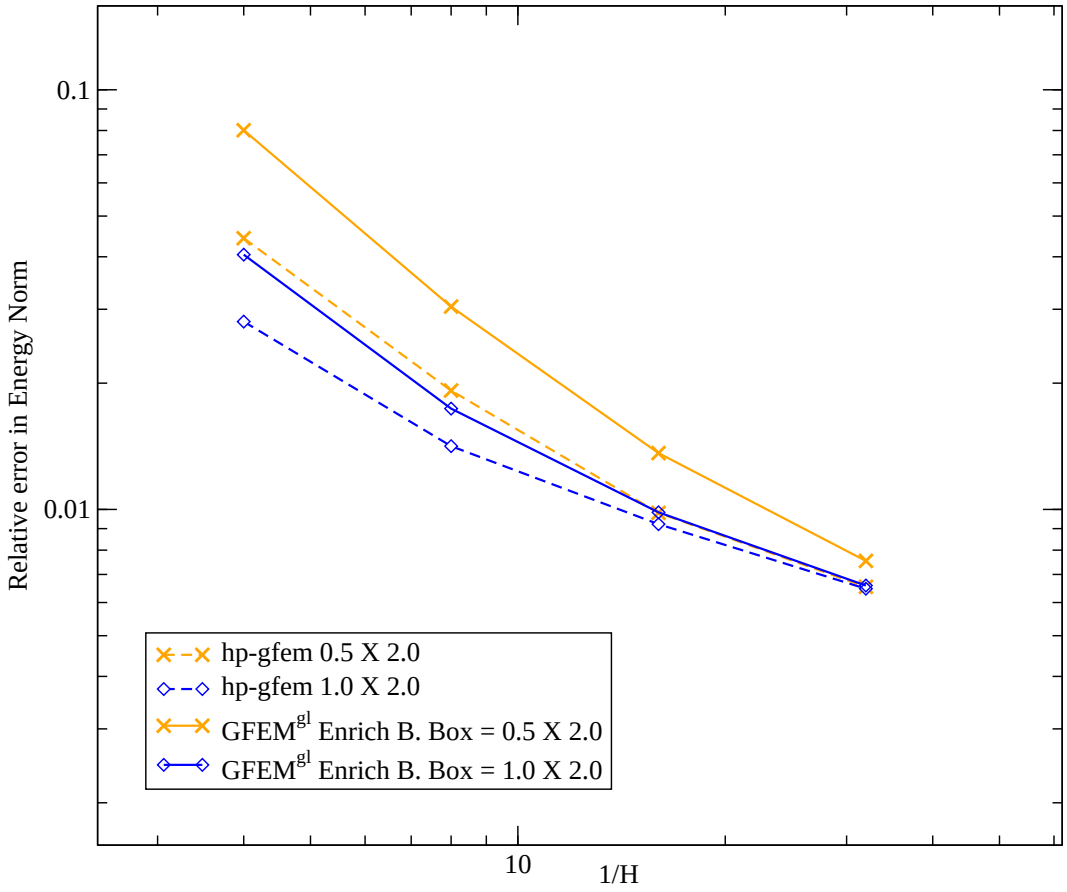

Figure 2.25: *Convergence plots showing hp-*GFEM *results and* GFEM$^{g\text{-}l}$ *results for 2 different enrichment zone sizes and local refinement zone sizes respectively.*

Chapter 3

Effect of inexact Boundary Conditions

This chapter deals with the effect of applying inexact Boundary Conditions on local problems. Since, in a general case, the boundary conditions for local problems would be obtained from the solution of an initial coarse scale (crude) global problem, $\boldsymbol{u}_G^0$, so they are only an approximation to the exact boundary conditions. As also discussed in Section 1.3, the bigger the local domain size, the better it would be in terms of using inexact boundary conditions for the local BVP from Saint Venant's Principle. However, this would also lead to higher computational costs. So, the issue of using inexact boundary conditions needs to be addressed, which will further help in ascertaining the size of the local domain.

In the context of the *GFEM*$^{g\text{-}l}$, there are various problems in which the boundary conditions applied on the local problem will not be exact. In static crack problems, the boundary conditions for the local problem will be obtained from the solution of the crude global problem in which the crack is not usually modeled; in the problems of crack growth [22], the boundary conditions for the local problem in the current crack step are provided from the solution of the previous crack step (as shown in Figure 3.1). The current study is focused on studying, the effect of inexact boundary conditions on the local problem arising due to this lag in crack size, with the help of theoretical and numerical results provided in the following sections.

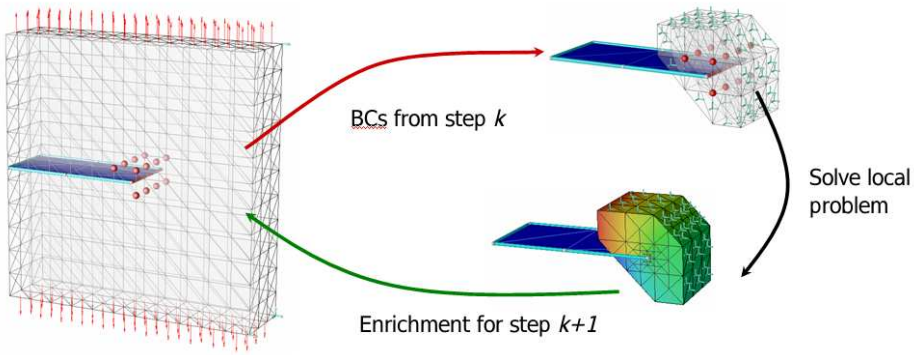

Figure 3.1: *Figure showing the process of solving a crack growth problem with the help of* GFEM$^{g\text{-}l}$*, where the BCs for local problem in step* $k+1$ *are obtained from the solution of global problem at step* k

3.1 Theoretical estimate of the Error in Boundary Condition

In Figure 3.2, the picture on left hand side shows a crack of size $2a$ lying in an infinite plate, loaded with tractions at infinity. With the help of symmetry, this problem can be studied as that of an edge-crack panel (similar to the one described in Chapter 2) with crack of size 'a' (location of crack tip being at $x = a$). Now, when the crack advances by a step size of Δa, the new location of the crack tip becomes $x = a + \Delta a$, with the size of crack being $2a + 2\Delta a$. The picture on the right-hand-side in Figure 3.2 shows the polar-coordinate system for two crack configurations (i.e. one at $x = a$ and the other at $x = a + \Delta a$). S_2 denotes the boundary of the local domain surrounding the crack tip located at $x = a + \Delta a$. The exact boundary conditions, which come from the asymptotic expansion of Mode I opening of the crack of size $2a + 2\Delta a$, is denoted by $\vec{u}_{a+\Delta a}$ in Equation (3.2). In $GFEM^{g\text{-}l}$ approach, the boundary conditions for S_2 will be provided from solution of the problem at previous crack step, in which the crack tip lies at $x = a$ (i.e. corresponding to domain S_1) and is given by $\vec{u}_a$ in Equation (3.1). The near crack-tip displacement field for crack size

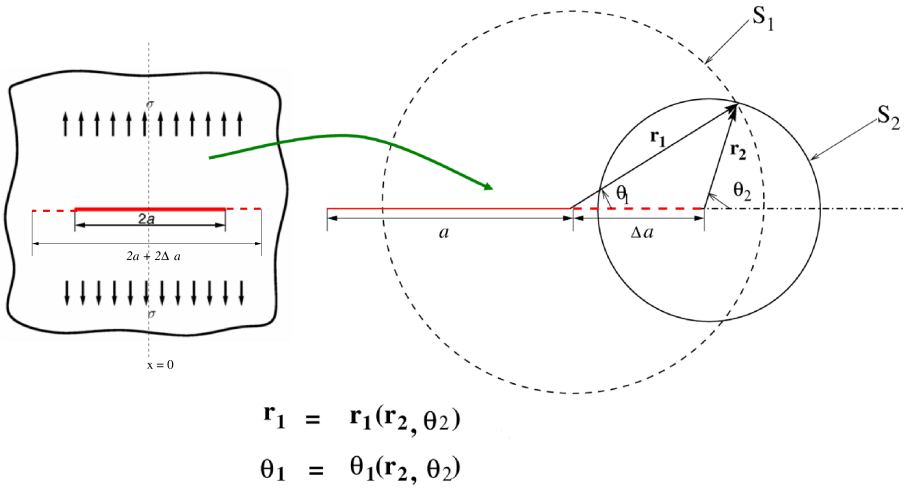

Figure 3.2: *Figure showing coordinate system representation for cracks of size (2a) and (2a + 2Δa) for an infinite plate loaded at infinity.*

$2a$, corresponding to the Mode I opening of the crack for plane strain problem is given by (higher terms omitted) [28]:

$$\vec{u}_a(r_1, \theta_1) = \frac{K_I^a}{G}\left[\frac{r_1}{(2\pi)}\right]^{\frac{1}{2}} \left\{ \begin{array}{l} \cos\frac{\theta_1}{2}\left[1 - 2\nu + \sin^2\frac{\theta_1}{2}\right] \\ \sin\frac{\theta_1}{2}\left[2 - 2\nu - \cos^2\frac{\theta_1}{2}\right] \end{array} \right\} \tag{3.1}$$

where,

K_I^a is the Mode I SIF for crack of size $2a$

'r_1' denotes distance of the point where we seek the solution, from crack tip

'G' is the shear modulus

'θ_1' is the angle from the horizontal reference axis as shown in Figure 3.2

'ν' is the Poisson's Ratio

Similarly, for the crack of size $2a+2\Delta a$, the displacement field is given by,

$$\vec{u}_{a+\Delta a}(r_2,\theta_2) = \frac{{K_I}^{a+\Delta a}}{G}\left[\frac{r_2}{(2\pi)}\right]^{\frac{1}{2}}\left\{\begin{array}{l}\cos\frac{\theta_2}{2}\left[1-2\nu+\sin^2\frac{\theta_2}{2}\right]\\ \sin\frac{\theta_2}{2}\left[2-2\nu-\cos^2\frac{\theta_2}{2}\right]\end{array}\right\} \tag{3.2}$$

Equation (3.2) represents the exact boundary conditions for the problem, whereas Equation (3.1) corresponds to the approximate boundary conditions. In Equation (3.1), r_1 and θ_1 can be written as functions of both r_2 and θ_2 by coordinate transformation and are given as follows,

$$\left.\begin{array}{l} r_1 = \sqrt{(\Delta a)^2 + 2(\Delta a) r_2 \cos\theta_2 + {r_2}^2} \\ \cos\theta_1 = \frac{\Delta a + r_2\cos\theta_2}{r_1} \\ \sin\theta_1 = \frac{r_2\sin\theta_2}{r_1} \end{array}\right\} \tag{3.3}$$

and therefore, $\vec{u}_a$ can be expressed as a function of r_2 and θ_2.

The error in boundary condition, because of the crack lag will be given by the difference of solution vectors in equations (3.2) and (3.1),

$$\vec{e}_{BC}(r_2,\theta_2) = \vec{u}_{a+\Delta a}(r_2,\theta_2) - \vec{u}_a(r_2,\theta_2) \tag{3.4}$$

Lets define the relative error in Boundary Condition (BC) in terms of a scalar quantity as,

$$e_r = \frac{\int_{-\pi}^{\pi}(\vec{e}_{BC}.\vec{e}_{BC})\, r_2\, d\theta_2}{\int_{-\pi}^{\pi}(\vec{u}_{a+\Delta a}.\vec{u}_{a+\Delta a})\, r_2\, d\theta_2} \tag{3.5}$$

where the quantity in the numerator is the integral of inner product of $\vec{e}_{BC}$ over S_2, and the quantity in the denominator is the integral of inner product of exact boundary condition, $\vec{u}_{a+\Delta a}$ over S_2.

To study the effect of crack step size Δa on the error in BC, crack step sizes ranging from 0 to 12 are used, with 3 different sizes of local domain, S_2: $r_2 = 9, 10$ and 11. The value of the Shear Modulus, G is taken equal to unity and a Poisson's ratio (ν) of zero is chosen. Also, to keep these theoretical estimates on the same ground as the numerical studies presented in the following section, the value of the SIF, K_I is kept as unity for all the cases; although K_I is a function of the magnitude of traction, σ (Figure 3.2) and crack size $2a$ ($K_I = \sigma\sqrt{\pi a}$), traction (σ) can be adjusted

according to the crack size to yield $K_I = 1.0$.

The relative error in BC, e_r (defined in Equation (3.5)) has been numerically evaluated for values of different parameters mentioned above with the help of a MATLAB code (only *x-component* of $\vec{e}_{BC}$ is taken into consideration here, because the expressions for *x* and *y-components* are very similar (Equation 3.1), both proportional to $\sqrt{r}$ and similar functions of θ). Figure 3.3 shows the variation of error in BC with the crack step size, Δa, plotted for three different

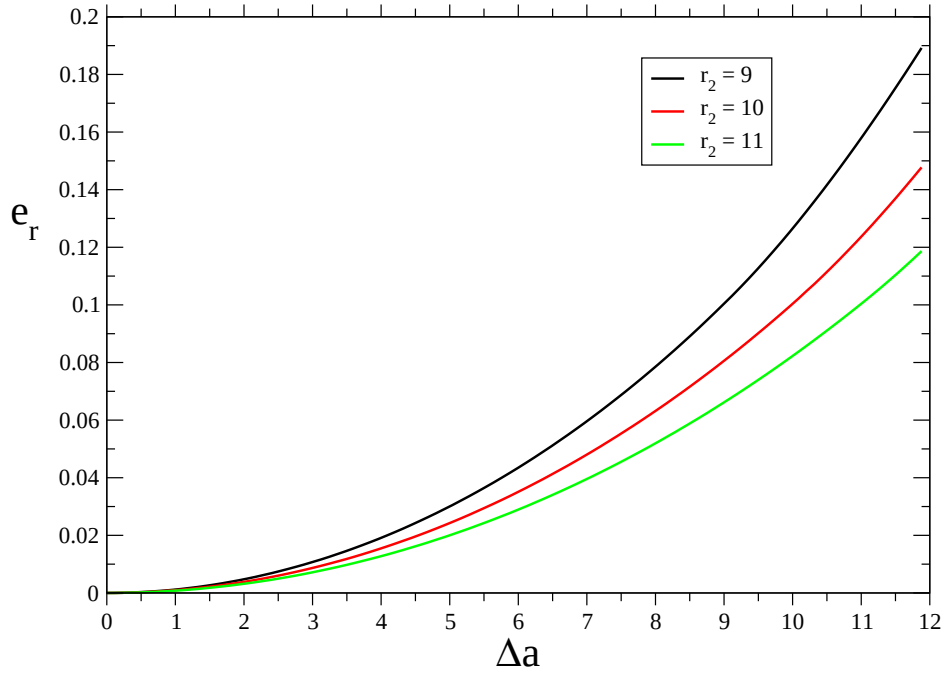

Figure 3.3: *Figure showing the variation of error in BC with the crack step size* Δa

sizes of local domain S_2 ($r_2 = 9, 10$ and 11). As can be seen from the figure, for all the three domain sizes, error grows up exponentially with crack step size, starting from no error for $\Delta a = 0$. Also, in agreement with Saint Venant's principle, lower error levels are observed for larger local domain size.

The same quantity, e_r is plotted again in Figure 3.4, but now against the crack step size (Δa) scaled with the size of local domain S_2 (r_2). All three curves (corresponding to three different sizes of local domain) overlap when plotted this way, showing the direct dependence of the relative error on the scaled parameter, $\frac{\Delta a}{r_2}$. This result, in particular, is encouraging because it can help in selecting the local domain size for a given crack step (Δa) and a desired error level, which instigates to further explore this on a problem of practical interest, and is the topic of next section.

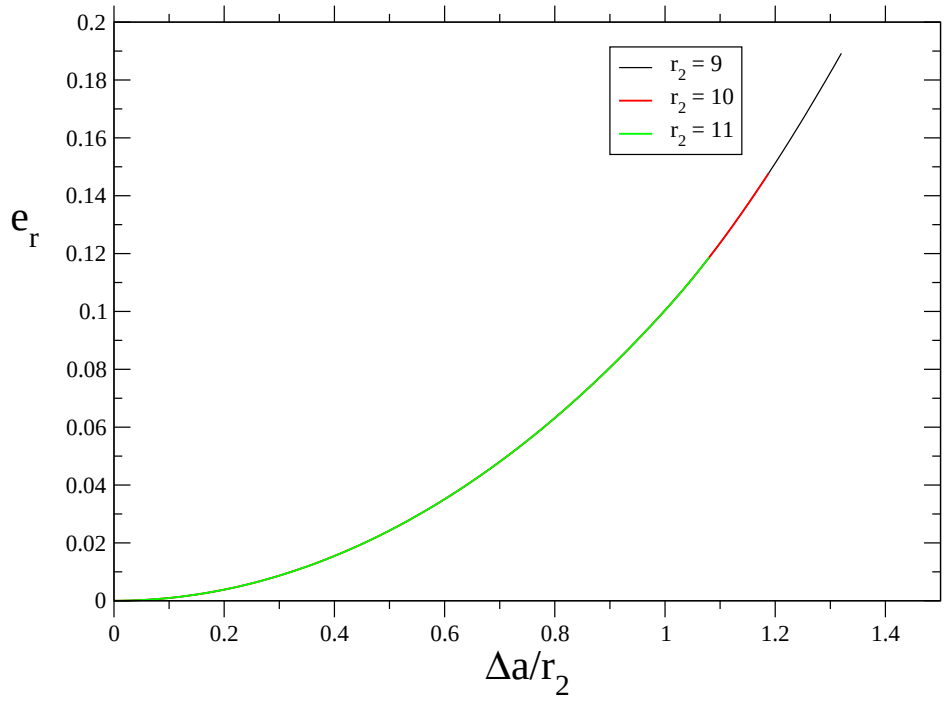

Figure 3.4: *Figure showing the variation of error in BC with crack step scaled by the size of* S_2 $\left(\frac{\Delta a}{r_2}\right)$

3.2 Numerical Studies and Discussion

This section deals with studying the effect of inexact Boundary Conditions due to crack lag on a finite, 3-D linear elastic Fracture Mechanics problem as shown in Figure 3.5. It is a square edge-crack panel with uniform thickness of 1” throughout. The value of Youngs Modulus is taken equal to unity. A Poissons ratio value of 0.0 is chosen because in that case it becomes a 2-D problem for which we know the exact solution in the entire domain of the problem, which can be used to apply the boundary conditions on the global as well as local problem. The boundary conditions are applied in the form of tractions derived from the first order term of asymptotic expansion of the Mode I opening of crack.

In this study, two different Boundary Conditions are applied on the same local problem domain (See Figure 3.6).

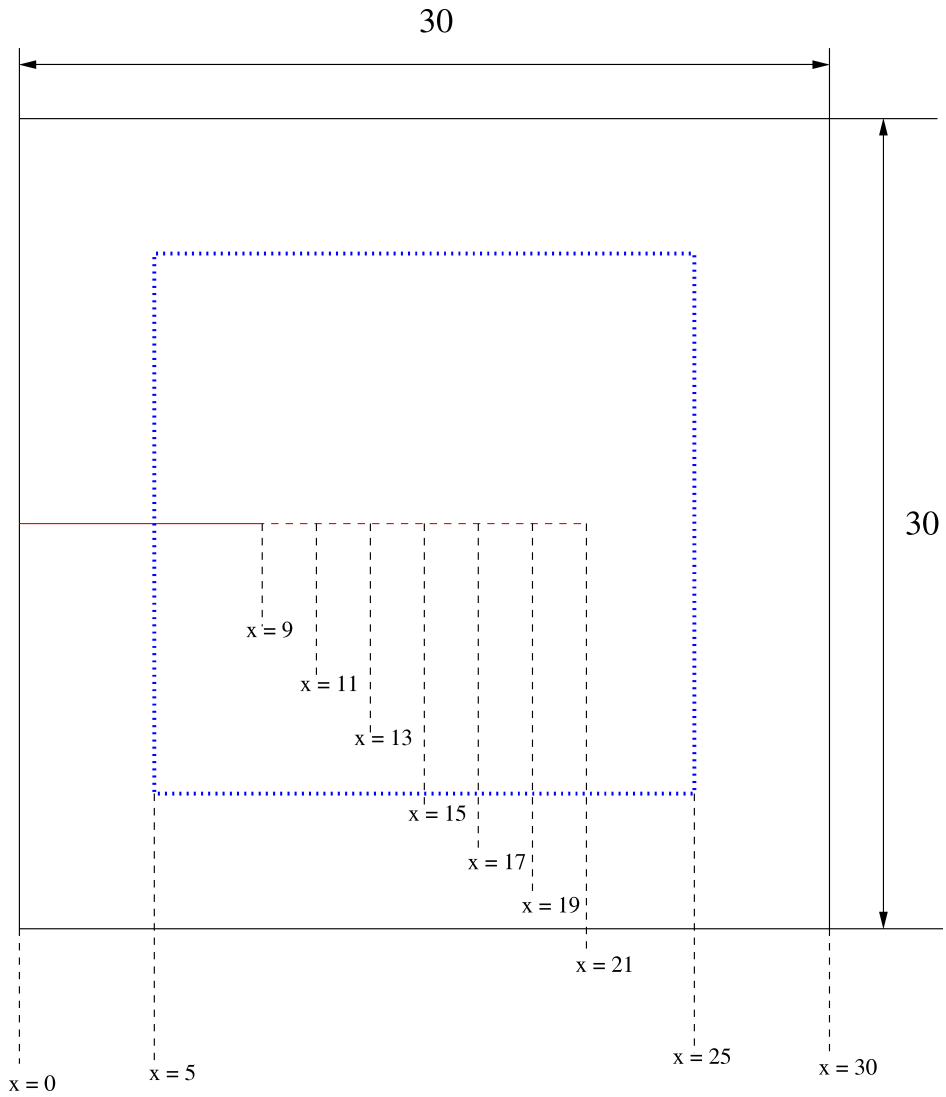

Figure 3.5: *Edge-crack panel showing different locations of crack front to study the effect of inexact Boundary Conditions*

The picture on the right-hand-side in Figure 3.6 shows the exact boundary conditions applied on the local problem domain with crack front location at $x = a + \Delta a$. The solution corresponding to this case provides the reference solution. On the other hand, the picture on the left shows the inexact boundary conditions, obtained from Mode I expansion corresponding to crack front location at $x = a$, applied on the same local problem domain. This would give the approximate solution obtained by applying the inexact boundary conditions on the local problem. Note that, both the reference solution and the approximate solution would also contain the Finite Element discretization errors, which are not taken into account in this study.

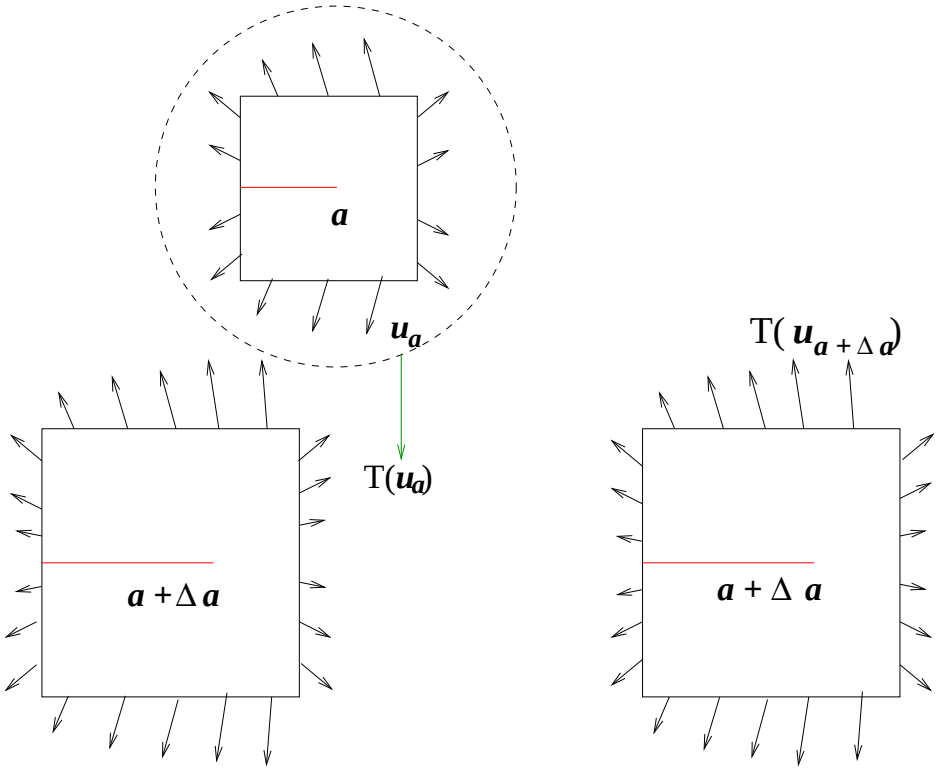

Figure 3.6: *Figure showing local problem domains solved with two different boundary conditions: The picture on left shows the one corresponding to the inexact boundary conditions and the right side picture shows the case corresponding to the exact boundary conditions on the local problem.*

The dotted blue square in Figure 3.5 shows the boundary of a local domain of size *20" X 20"*. The dashed lines show different locations of the crack front used in this study. The point where the solid red line ends ($x = 9$), indicates the position of the crack front, Mode I asymptotic expansion from which is used to apply the inexact boundary conditions. These inexact boundary conditions arise due to crack lag on the local problems with different crack front locations as marked in the figure. This leads to the different crack step sizes, Δa. For example, when a problem with the crack front location of $x = 15$ is solved, the reference solution is obtained by applying exact boundary conditions

from asymptotic expansion of Mode I opening of the crack corresponding to crack front location of $x = 15$. On the other hand, the Mode I asymptotic expansion corresponding to crack front location of $x = 9$ is used to apply inexact boundary conditions on the local problem ($\Delta a = 15" - 9" = 6"$). Note, that in both the cases, the boundary conditions applied on the enriched global problem are exact (i.e. from the solution corresponding to crack front location of $x = 15$), because this study aims to investigate the effect of applying wrong boundary conditions only on the local problem.

So, for each crack front location, $x = 11, 13, 15, 17, 19, 21$ and respective crack step size, $\Delta a = 2, 4, 6, 8, 10, 12$, there is a reference $GFEM^{g\text{-}l}$ solution obtained by applying the exact boundary conditions and there is a solution obtained by applying inexact boundary conditions from Mode I asymptotic expansion corresponding to crack front location at $x = 9$. The difference between the two provides the error due to inexact boundary conditions applied on the local problem. In this study, relative errors in strain energy of the local and global problems have been computed and compared.

The relative error in strain energy of the local problem is given as,

$$e_r^{loc} = \frac{\left| U_L^{exactBC} - U_L^{inexactBC} \right|}{U_L^{exactBC}} \tag{3.6}$$

where, $U_L^{exactBC}$ and $U_L^{inexactBC}$ denote strain energy of the local problem obtained from the solution of problems shown on right-hand-side and left-hand-side respectively, in Figure 3.6.

Similarly, the relative error in strain energy of the enriched global problem is given by,

$$e_r^{EG} = \frac{\left| U_{EG}^{exactBC} - U_{EG}^{inexactBC} \right|}{U_{EG}^{exactBC}} \tag{3.7}$$

The Finite Element simulations in this study are performed using *ISET* (Section 2.3). The global problem has a single through-the-thickness crack and is discretized with a uniform mesh of tetrahedral elements, with only one layer of elements being provided in the z-direction. The crack has been modeled with the help of discontinuous step-function enrichments given in [24]. Figure 3.7 shows the initial global mesh used for this study in the picture on left-hand side. The local problem has been extracted from the blue square region in the global mesh and the local mesh is shown in the picture on right-hand-side. The local mesh is generated by performing *8* levels of crack front refinement ($nref_{front} = 8$), to capture the singularity better. Also, in this study, geometrical enrichment has been used and the size of enrichment zone is the same as the local problem domain.

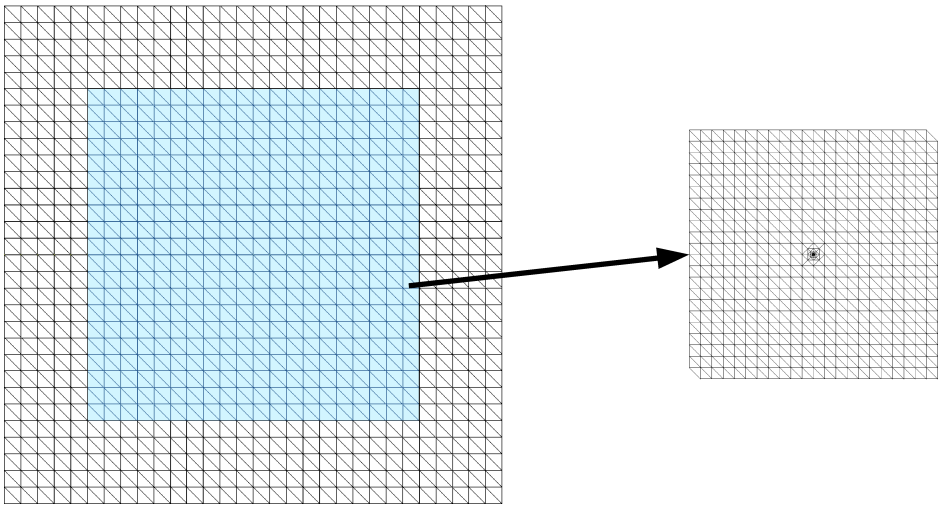

Figure 3.7: *Figure showing the global and local problem meshes used for studying the effect of inexact Boundary Conditions*

Results: Figure 3.8 shows relative error in strain energy of the local problem plotted against the crack step size Δa for different local problem domain sizes. These local problem domains are equivalent to the ones used in Section 3.1, in the sense that radius (r) of the circles, inscribed in these square local problem domains are equal to r_2 used in Section 3.1. As can be seen from the plots, the relative error increases exponentially with the crack step size and very high error levels (relative error of more than *100*) are observed for larger crack steps. Also, lower error levels are observed for larger local domains. The behavior of these error plots is very similar to the ones obtained by theoretical estimates in Figure 3.3.

Further, this relative error in strain energy is plotted against a scaled parameter, $\frac{\Delta a}{r}$, similar to Figure 3.4. Figure 3.9 shows a similar trend as seen in theoretical estimates (Section 3.1), and the three curves (corresponding to the 3 local domain sizes) are almost overlapping on each other.

Now, lets see how these inexact BCs on the local problem affect the solution in the Enriched Global problem. Figures 3.10 and 3.11 show the plots of Relative error in Strain Energy of the Enriched Global problem against Δa and $\frac{\Delta a}{r}$ respectively. The plots show the similar nature of the curves, as seen in the local problem as well as in the theoretical estimates. An important point though, is the error levels are 5 orders of magnitude lesser than that observed in the case of local problem (Figure 3.8). This also, clearly shows the advantage of going one step further in global-local analysis and solving the global problem again by using the solution of local problem as enrichments. Even though, the error levels in Enriched Global Problem are insignificant in this case but, knowing the trend in variation of relative error with the crack step size can help a great deal in selecting the local domain size, for a given crack step (Δa) and a desired error level, in cases wherein error levels due to wrong Boundary Conditions might get significant.

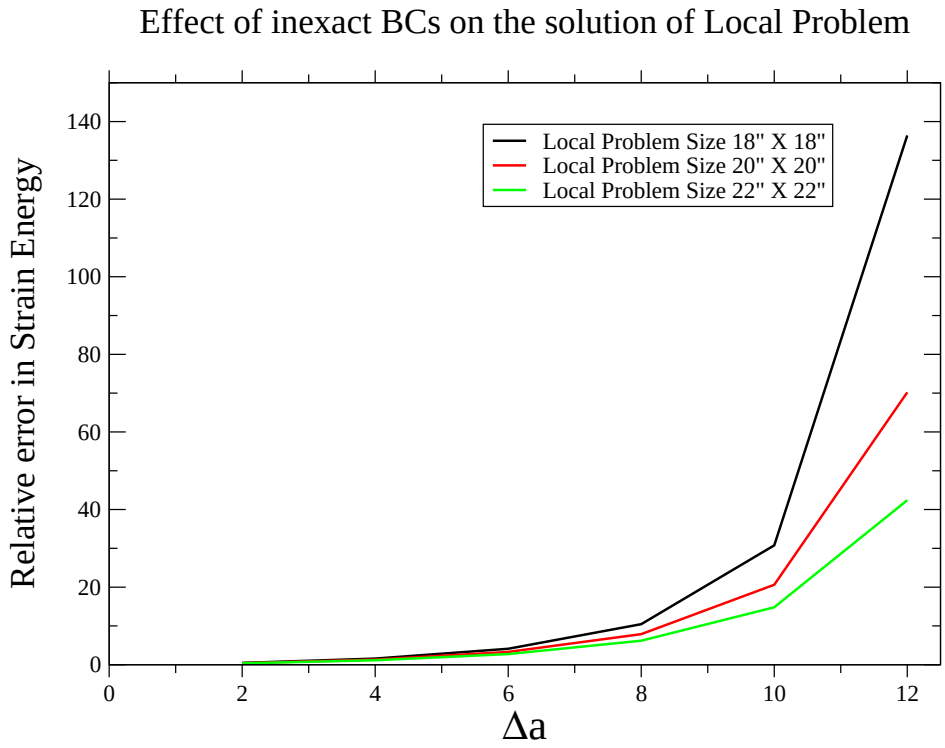

Figure 3.8: *Figure showing the relative error in Strain Energy of Local Problem plotted against crack step size Δa*

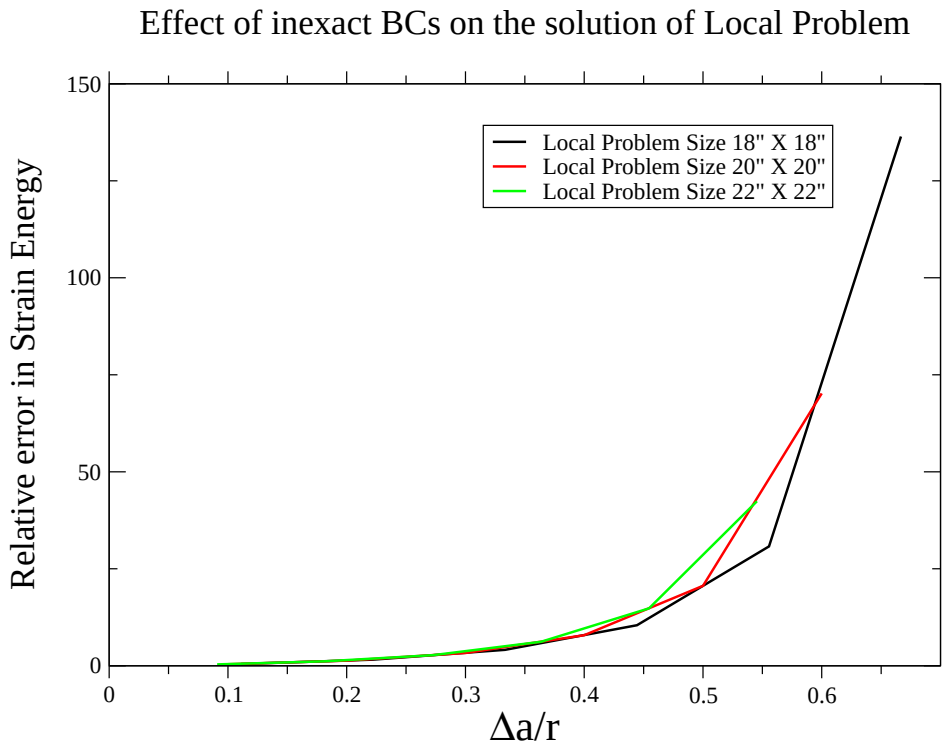

Figure 3.9: *Figure showing the relative error in Strain Energy of Local Problem plotted against a scaled parameter,* $\frac{\Delta a}{r}$

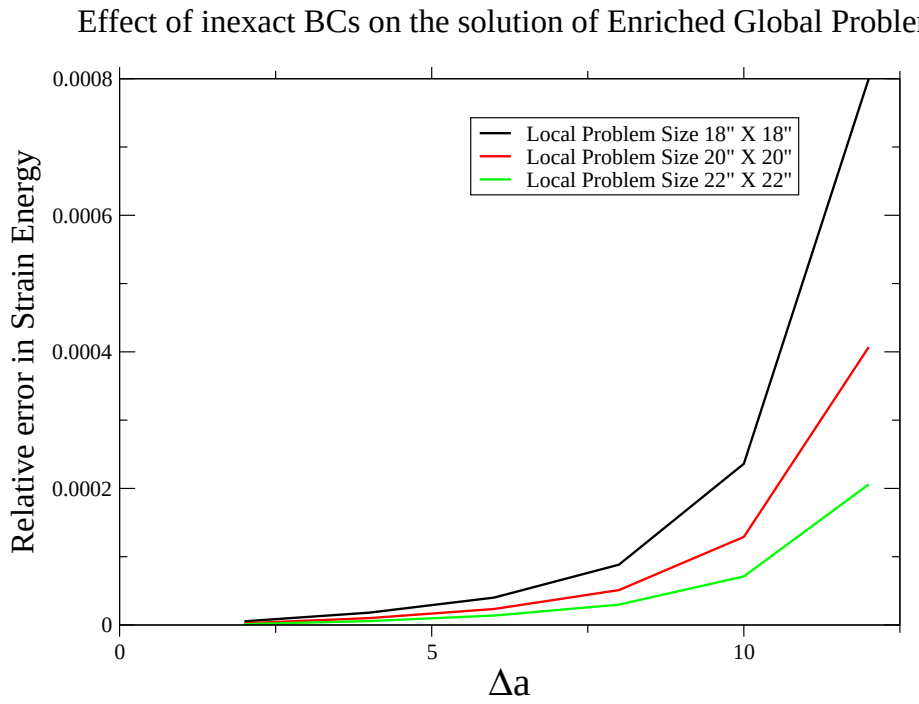

Figure 3.10: *Figure showing the relative error in Strain Energy of Enriched Global Problem plotted against crack step size Δa*

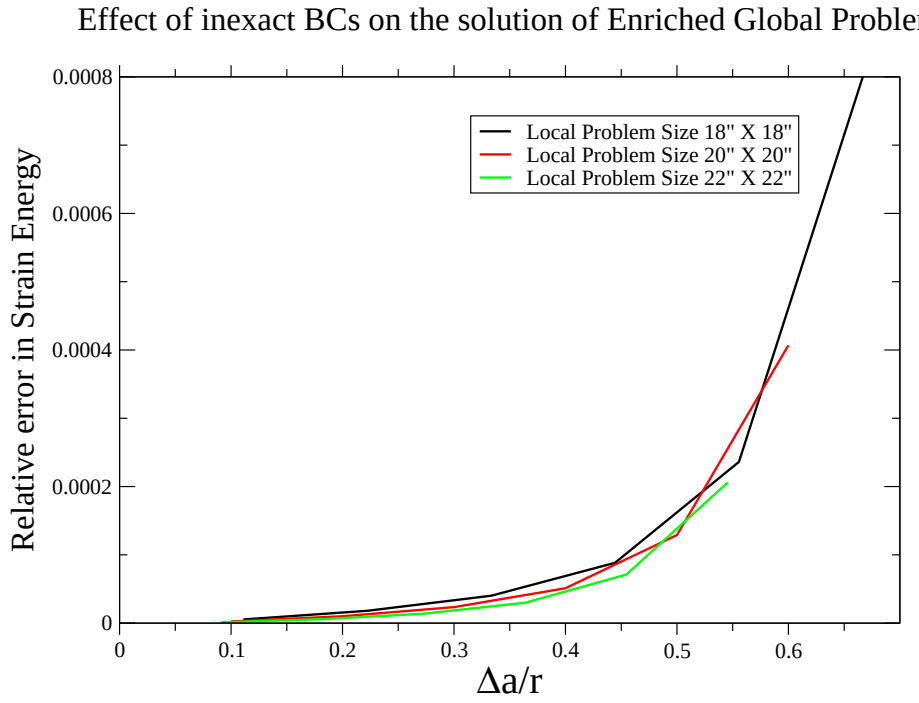

Figure 3.11: *Figure showing the relative error in Strain Energy of Enriched Global Problem plotted against* $\frac{\Delta a}{r}$

Chapter 4

Concluding Remarks

This study is focused on the issues related to Generalized Finite Element Method with Global-Local enrichments (*GFEM*$^{g\text{-}l}$), in which the solution of a Local Boundary Value Problem consisting of localized features like crack, inclusions, etc. is used to enrich the global solution space. In this research, the following two major issues related to these methods are addressed: (i) Size of Enrichment Zone (Chapter 2) and (ii) Effect of Inexact Boundary Conditions on the Local Problem (Chapter 3). These two factors in turn, can help us providing the guidelines to select the size of local domain. The results and conclusions drawn from this study can be summarized as follows:

- We have seen from the results in Chapter 2, as the size of local refinement region (in *hp-GFEM*) or that of enrichment zone (in *GFEM*$^{g\text{-}l}$) is increased, convergence rates improve.
- The theoretical estimate for the size of enrichment zone given by Equation (2.11), can be used to guide the size of the enrichment zone in Generalized Finite Element Methods for Fracture Mechanics problems.
- The role of the enrichment zone in *GFEM*$^{g\text{-}l}$ is similar to that of local refinement region in *hp-GFEM*.
- The already existing rules of thumb used in industry for guiding the optimal *h*- and *p*- distribution in *hp-GFEM* can also be used to guide the discretization strategy for local problem mesh in *GFEM*$^{g\text{-}l}$.
- For the Mode I crack opening problem, the inexact boundary conditions due to crack lag on the local problem do not affect the Enriched Global Problem significantly, and the magnitude of error levels in the Enriched Global Problem are seen to be of 5 orders of magnitude lower than that in the Local Problem itself.
- For the problems, where error levels because of wrong Boundary Conditions become significant in the Enriched Global Problem as well, the knowledge of trend in variation of relative error with crack step size (as seen in Chapter 3) can come in handy to select the local domain size for a given crack step and a desired error level. This is also going to be author's continued work in his doctoral research.

Chapter 5

References

[1] D. N. Arnold, A. Mukherjee, and L. Pouly. Locally adapted tetrahedral meshes using bisection. *SIAM Journal of Scientific Computing*, 22(2):431–448, 2000.

[2] I. Babuška and J.M. Melenk. The partition of unity finite element method. *International Journal for Numerical Methods in Engineering*, 40:727–758, 1997.

[3] I. Babuška, G. Caloz, and J.E. Osborn. Special finite element methods for a class of second order elliptic problems with rough coefficients. *SIAM Journal on Numerical Analysis*, 31(4):945–981, 1994.

[4] E. Bansch. Local mesh refinement in 2 and 3 dimensions. *Impact of Computing in Science and Engineering*, 3: 181–191, 1991.

[5] E. Béchet, H. Minnebo, N. Moës, and B. Burgardt. Improved implementation and robustness study of the x-fem for stress analysis around cracks. *International Journal for Numerical Methods in Engineering*, 64:1033–1056, 2005.

[6] T. Belytschko and T. Black. Elastic crack growth in finite elements with minimal remeshing. *International Journal for Numerical Methods in Engineering*, 45:601–620, 1999.

[7] C.A. Duarte. *The hp Cloud Method*. PhD dissertation, The University of Texas at Austin, December 1996. Austin, TX, USA.

[8] C.A. Duarte and D.-J. Kim. Analysis and applications of a generalized finite element method with global-local enrichment functions. *Computer Methods in Applied Mechanics and Engineering*, 197(6-8):487–504, 2008. http://dx.doi.org/10.1016/j.cma.2007.08.017.

[9] C.A. Duarte, I. Babuška, and J.T. Oden. Generalized finite element methods for three dimensional structural mechanics problems. *Computers and Structures*, 77:215–232, 2000.

[10] C.A.M. Duarte and J.T. Oden. Hp clouds–A meshless method to solve boundary-value problems. Technical Report 95-05, TICAM, The University of Texas at Austin, May 1995.

[11] C.A.M. Duarte and J.T. Oden. *Hp* clouds – An *hp* meshless method. *Numerical Methods for Partial Differential Equations*, 12:673–705, 1996.

[12] C.A.M. Duarte and J.T. Oden. An *hp* adaptive method using clouds. *Computer Methods in Applied Mechanics and Engineering*, 139:237–262, 1996.

[13] I. Hirai, B.P. Wang, and W.D. Pilkey. An efficient zooming method for finite element analysis. *International Journal for Numerical Methods in Engineering*, 20:1671–1683, 1984.

[14] D.-J. Kim, J.P. Pereira, and C.A. Duarte. Analysis of three-dimensional fracture mechanics problems: A two-scale approach using coarse generalized FEM meshes. *International Journal for Numerical Methods in Engineering*, 81(3):335–365, 2010. http://dx.doi.org/10.1002/nme.2690.

[15] Dae-Jin Kim. *The Generalized Finite Element Method with Global-Local Enrichment Functions*. PhD thesis, University of Illinois at Urbana-Champaign, 2009.

[16] P. Laborde, J. Pommier, Y. Renard, and M. Salaün. High-order extended finite element method for cracked domains. *International Journal for Numerical Methods in Engineering*, 64:354–381, 2005.

[17] J.M. Melenk and I. Babuška. The partition of unity finite element method: Basic theory and applications. *Computer Methods in Applied Mechanics and Engineering*, 139:289–314, 1996.

[18] N. Moës, J. Dolbow, and T. Belytschko. A finite element method for crack growth without remeshing. *International Journal for Numerical Methods in Engineering*, 46:131–150, 1999.

[19] J.T. Oden, C.A. Duarte, and O.C. Zienkiewicz. A new cloud-based *hp* finite element method. *Computer Methods in Applied Mechanics and Engineering*, 153:117–126, 1998.

[20] P. O'Hara, C.A. Duarte, and T. Eason. Generalized finite element analysis of three-dimensional heat transfer problems exhibiting sharp thermal gradients. *Computer Methods in Applied Mechanics and Engineering*, 198 (21-26):1857–1871, 2009. http://dx.doi.org/10.1016/j.cma.2008.12.024.

[21] K. Park, J.P. Pereira, C.A. Duarte, and G.H. Paulino. Integration of singular enrichment functions in the generalized/extended finite element method for three-dimensional problems. *International Journal for Numerical Methods in Engineering*, 78(10):1220–1257, 2009. http://dx.doi.org/10.1002/nme.2530.

[22] J. P. Pereira. *Generalized Finite Element Methods for three-dimensional crack growth simulations*. PhD thesis, University of Illinois at Urbana-Champaign, 2010.

[23] J.P. Pereira and C.A. Duarte. Extraction of stress intensity factors from generalized finite element solutions. *Engineering Analysis with Boundary Elements*, 29:397–413, 2005.

[24] J.P. Pereira, C.A. Duarte, D. Guoy, and X. Jiao. *Hp*-Generalized FEM and crack surface representation for non-planar 3-D cracks. *International Journal for Numerical Methods in Engineering*, 77(5):601–633, 2009. http://dx.doi.org/10.1002/nme.2419.

[25] Marc Alexander Schweitzer. Stable enrichment and local preconditioning in the particle-partition of unity method. sfb611.iam.uni-bonn.de/uploads/380-komplett.pdf.

[26] T. Strouboulis, K. Copps, and I. Babuška. The generalized finite element method. *Computer Methods in Applied Mechanics and Engineering*, 190:4081–4193, 2001.

[27] B. Szabo and I. Babuška. *Finite Element Analysis*. John Wiley and Sons, New York, 1991.

[28] H. Tada, P. Paris, and G. Irwin. *The Stress Analysis of Cracks Handbook*. ASME Press, New York, 3rd edition, 2000.

[29] J.D. Whitcomb. Iterative global/local finite element analysis. *Computers and Structures*, 40:1027–1031, 1991.